![UiA University of Agder logo]

ENE500-G

Master's Thesis Renewable Energy

Grounding and Charging Strategy for Ships during Cold Ironing Operation

MARIA KOLBERG BENDEN

SUPERVISORS:

Immanuel Ninma Jiya,

van Khang Huynh,

and Milad Golzar

University of Agder, 2022

Faculty of Engineering and Science

Department of Engineering Science

May 16, 2022

Abstract

In order to minimize the pollution that ships generate at ports, ships can be connected to the utility grid during charging, also known as shore-to-ship connection or cold ironing operation. The pollution can also be remarkably reduced if the ships are full-electric or hybrid. With the utilization of a common DC bus, several ships can be charged simultaneously. However, due to the common DC bus, the ships are not galvanic isolated from each other such that leakage current can occur among the ships and the quay when the current leaks to the ground during a fault. Hence, this paper proposes a complete charging and grounding strategy, which will provide galvanic isolation between the ships and the quay. The charging and grounding strategy are verified through simulations in the Matlab/Simulink environment. An isolated and ideal PSFB DC-DC converter with a rated power of 400 kW was proposed to obtain galvanic isolation. The proposed converter obtained a stable output during nominal and half load from the simulation results. In addition, two grounding systems on the shore-side and the ship-side were proposed. On the shore-side, a double grounding TN-C grounding system with a NGR resistor was designed such that the leakage current can easily be detected when a ground fault occurs. On the ship-side, an IT system with HRMG resistors was designed to reduce the leakage current such that the risk of corrosion was reduced and provided safety for personnel. As a result, a fault on the shore-side did not affect the ship-side grounding system and opposite. Faults that can appear on the charging system were found through research and simulated with the complete charging and grounding system to verify that the grounding system was optimally designed. The results during a fault on the system showed that the shore-side grounding system was not optimally designed because the NGR did not reduce the fault current to a lower value than 25 A. The common DC bus was created from an uncontrolled rectifier that suffered a substantial power dissipation. As a result, the output of the PSFB DC-DC converter was unstable. Therefore, a resistor was added to the TN-C grounding configuration during simulations of the charging system to achieve a stable output of the DC-DC converter. The IT grounding configuration on the ship-side reduced the fault current to 6 mA during a LG fault, and personnel safety was kept at a safe level when a person touched one of the DC lines. However, it was shown that the personnel safety was not obtained when a person touched the energized chassis due to a dangerous voltage potential.

Preface

This master thesis was created during the spring semester of 2022 at the University of Agder in Grimstad. The scope of the study is 30 study points and is the concluding task for the master's study in Renewable Energy. During my five years at the university, great and broad knowledge about renewable energy has also made me aware why it is so crucial that renewable energy sources must phase out fossil fuel sources to reduce climate change. Therefore, I hope that the expertise I have gained about renewable energy can come in handy in my working career.

While writing my master's thesis, I was informed about why it is so important to be able to charge ships with the utility grid as well as get the ships to run on electricity. These ships are facing issues today due to corrosion phenomena, which has been an inspiring task. I have never learned anything about grounding systems, which has helped me understand the importance of a proper grounding configuration. I hope that my work this semester will help Blue Day Technology will solve some of the problems they are handling today. In addition, I hope my work can be helpful for further learning for students at the University of Agder.

I want to give a great thanks to Immanuel Ninma Jiya for helping and guiding me on the right way during the whole semester and has always been available if there was anything that I was unsure of. Besides, I would like to thank van Khang Huynh for the guidance and feedback during the guidance meetings. I would also like to thank the persons in Blue Day Technology; Milad Golzar, Morten Skogseth, and Hans Petter Heggebø, for giving advice and answering if there was anything that I was wondering.

A great thanks to the University of Agder for giving me five very good years here in Grimstad.

Individual Mandatory Declaration

The individual student or group of students is responsible for the use of legal tools, guidelines for using these and rules on source usage. The statement will make the students aware of their responsibilities and the consequences of cheating. Missing statement does not release students from their responsibility.

1.	I/We hereby declare that my/our report is my/our own work and that I/We have not used any other sources or have received any other help than mentioned in the thesis.	☒
2.	I/we further declare that this thesis: - has not been used for another exam at another department/university/university college in Norway or abroad; - does not refer to the work of others without it being stated; - does not refer to own previous work without it being stated; - have all the references given in the literature list; - is not a copy, duplicate or copy of another's work or manuscript.	☒
3.	I/we am/are aware that violation of the above is regarded as cheating and may result in cancellation of exams and exclusion from universities and colleges in Norway, see Universitets- og høgskoleloven §§4-7 og 4-8 og Forskrift om eksamen §§ 31.	☒
4.	I/we am/are aware that all submitted theses may be checked for plagiarism.	☒
5.	I/we am/are aware that the University of Agder will deal with all cases where there is suspicion of cheating according to the university's guidelines for dealing with cases of cheating.	☒
6.	I/we have incorporated the rules and guidelines in the use of sources and references on the library's web pages.	☒

Publishing Agreement

Authorization for electronic publishing of the thesis.

Author(s) have copyrights of the thesis. This means, among other things, the exclusive right to make the work available to the general public (Åndsverkloven. §2).

All theses that fulfill the criteria will be registered and published in Brage Aura and on UiA's web pages with author's approval.

Theses that are not public or are confidential will not be published.

I hereby give the University of Agder a free right to

make the task available for electronic publishing: ☒JA ☐NEI

Is the thesis confidential? ☐JA ☒NEI

 (confidential agreement must be completed and signed by the Head of the Department)

  - If yes:

Can the thesis be published when the confidentiality period is over? ☒JA ☐NEI

Is the task except for public disclosure? ☐JA ☒NEI

(contains confidential information. see Offl. §13/Fvl. §13)

Contents

List of Figures

List of Tables

Nomenclature

AI Artificial Intelligence

CMC Common-Mode-Current

CMV Common-Mode Voltage

CSA Cross-Sectional Area

Cu Copper

DAB Dual-Active-Bridge

DCCB DC Circuit Breaker

EBC Equipotential Bonding Connection

ECP Exposed Conductive Part

EV Electrical Vehicle

FB Full-Bridge

FFT Fast Fourier Transform

HF High-Frequency

HR High Resistance

HRG High Resistance Grounding

HRMG High-Resistance Midpoint Grounding

HV High Voltage

HVSC High Voltage Shore Connection

ICCP Impressed Current Cathodic Protection

IMD Insulation Monitoring Device

LG Line-to-Ground

LL Line-to-Line

LR Low Resistance

LRG Low Resistance Grounding

LV   Low-Voltage

MG   Microgrid

ML   Machine Learning

MOSFET Metal-Oxide-Semiconductor Field-Effect Transistor

N   Neutral

NGR   Neutral Ground Resistor

PE   Protective Earth

PEN   Protective Earth Neutral

PF   Power Factor

PHEV Plug-in Electrical Vehicle

PSFB Phase-Shifted Full-Bridge

PWM Pulse-Width-Modulation

SiC   Silicon Carbide

TF   Transformer

VSC   Voltage Source Converter

WT   Wavelet Transform

1 Introduction

1.1 Background

DC-distributed charging stations for ships during cold ironing operation are often built up by step-down TFs and power converters. The AC power is sent through AC/DC conversion, filter, TF, filter, and AC/DC conversion. Such systems are bulky and expensive to build. As an alternative, the power can be sent via a common DC bus, as shown in figure 1. Besides, the costs and size will be reduced. However, the charging ships are no longer galvanic isolated from each other; if a leakage current from the grounding system flows in the seawater between the ships, a voltage potential arises between them. As a consequence, the corrosion accelerates and reduces the overall safety. A current of mA-range can contribute to considerable damage, and the challenge is identifying and locating such a small current. Therefore, the corrosion issue during cold ironing operation is significant to investigate further such that a proper charging and grounding strategy can be obtained. Blue Day Technology informed about the corrosion issue during charging.

In the course ENE-503, grounding strategies for shore-to-ship connection were investigated through research. From the previous course, the TN-island grounding system was suggested as a solution for the company's problem with corrosion issues. However, the company had tested this grounding system before on their ships without solving the corrosion problem. Therefore, a new grounding strategy will be further investigated and proposed in this paper. Moreover, to provide galvanic isolation between the ships, an isolated PSFB DC-DC converter was designed based on literature research and tested through simulations in the Matlab/Simulink environment. However, the design of the PSFB DC-DC converter was not optimal when the converter operated at half load. Hence, a new design of the converter will be proposed in this paper. When the course ENE-503 was completed, there was an agreement to design a complete charging and grounding system.
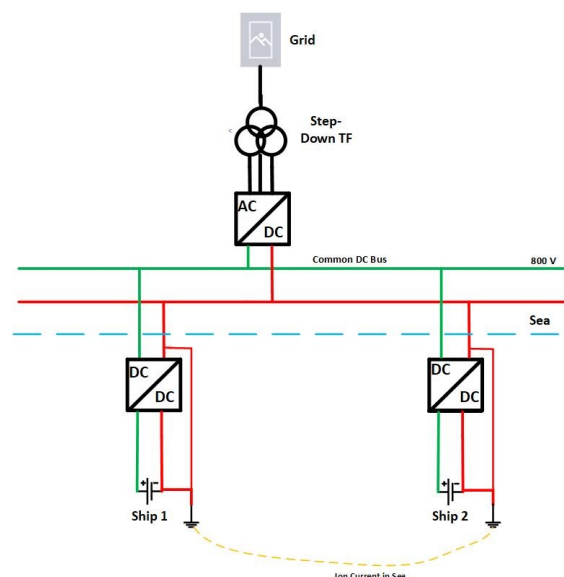
Figure 1: Blue Day Technology's approach to DC-distributed charging station for ships

Greenhouse gases from ships have a remarkable impact on global climate changes and public health. The pollution of fossil fuels from the transport sector contributes to the greenhouse effect, which will result in enormous consequences on Earth. Global warming that exceeds 1.5 °C will activate high sea levels and several types of catastrophes, such

as large storms, extreme drought, and forest fires. Besides, the weather catastrophes are estimated to be much worse than the world is handling today[6]. To a study by International Maritime Organisation, the maritime sector emits 940 million tonnes of CO2 annually, which contributes to between 2.5% and 3.0% of the global greenhouse gas emissions[7]. In order to find an alternative path to fossil fuels, the maritime sector has been working on several solutions. One solution includes hybrid and all-electric ships powered by rechargeable lithium-ion batteries, which are substantially utilized in the EV sector. In addition, if the batteries are charged with electrical power from the utility grid instead of diesel generators, the local emissions will also be remarkably reduced. The air quality at the port and noise reduction will be improved when shutting down the diesel generators[1].

AC started replacing DC at the end of the nineteenth century in power distribution. The main reason for this was that AC could be more easily transformed between different voltage levels and transmitted over longer distances, particularly in a cable transmission system. Today, DC power systems are restricted to particular applications, such as EVs, telecommunication systems, traction equipment, shipboard systems, and power transmission (HVDC). By comparing AC and DC powered systems, the DC system has advantages of long transmission distance, low transmission loss, high transmission capacity, ability to isolate DC faults, and accessibility of renewable energy. Based on these advantages, although the application of DC power distribution systems is just starting up, it is promising and worth studying[8].

The main challenge with a DC distributed system is when a fault occurs in the system. The fault current can increase to more than hundred times the nominal current during a sudden fault. In addition, a DC system does not have a natural zero-crossing point, which is a principal mechanism in an AC electrical CB rely for arc extinction and eventually fault isolation.
A DC distributed system must therefore be designed with regards to safety as well. Therefore, essential aspects must be taken into account for an optimal DC grounding structure. A fast and efficient fault detection strategy, a fault current limiting method, minimization of leakage current during normal and fault conditions, a proper DCCB, and maintaining the safety of equipment and personnel during a fault is crucial[9]. Hence, the DC grounding structure must therefore be investigated deeply.

1.2 Research Questions

The corrosion issue on the ships hull during cold ironing operation has lead to the following research questions:

- Which charging structure can be designed and utilized to provide galvanic isolation between the ships?
- Which grounding configuration should be utilized and designed to reduce and prevent corrosion between the ships under normal and fault conditions?
- Identify and simulate faults that can appear on the charging structure and investigate how the identified faults affect the chosen grounding and charging strategy.

1.3   Constraints and Important Notifications

In this paper, constraints have been taken into consideration to perform this study, and the limitations will be described further.

In a grounded electrical system, there are many different safety factors and standardization that need to be taken considered. CBs, fault detection strategies and insulation materials on the different components of a power system are among the most significant safety aspects. However, this paper has not implemented these factors in the designed charging and grounding system. In reality, they would have shut down the power system as quickly as possible if a fault had occurred on the electrical system. Only the insulation resistance of a battery pack has been considered in the system. The theory section has mentioned a short overview of existing fault detection strategies and DCCBs.

Even though a controlled AC/DC converter should have been used to obtain a stable DC bus voltage, and uncontrolled diode bridge rectifier has been considered in this paper.

Furthermore, even though there are three types of ground fault categories, only a simulation with a fixed time period has been contemplated and simulated. In addition, it has not been considered that the PSFB DC-DC converter shall obtain ZVS for achieving a higher level of efficiencies, such that leakage inductance neither magnetizing inductances nor resistances has been taken into account.

HV, MV, and LV are defined with different voltage ratings. In this paper, the DC system is operating with a rated voltage of 1000 V_{dc}, such that the DC electrical system is defined as a MV system, as in [10]. In the AC system, the system contains both HV and LV; HV is on the primary side of the TF. On the secondary side, the TF is operating with a voltage less than 1000 V and therefore defined LV, as in[11].

1.4   Outline of the Thesis

This thesis is divided into the following sections, excluding the introduction:

- Section 2 - in this section, a theoretical background will be presented. Relevant information and literature review regarding grounding and corrosion issues during cold ironing operation will be described. Theory about existing grounding systems and theory and literature review about grounding equipment for AC and DC-powered systems will be described. Faults in AC and DC distributed systems and impacts on DC grounding will also be given. Relevant theory and literature review regarding the two converters will be presented. The PSFB DC-DC converter contains a control system, so PID control will also be described. This section will also present the insulation resistance of a battery pack and relevant safety standards.
- Section 3 - The method for the created charging and grounding strategy during cold ironing operation will be described.
- Section 4 - the simulation results and discussion of the charging and grounding strategy will be presented.
- Section 5 - A summary and a conclusion will be remarked in this section.
- Section 6 - further recommendations is proposed in this section.

2 Theory

This paper is an extension of the unpublished work from the course ENE-503, titled "Charging Solution for Ships" by M.K. Benden[12]. In this theory section, the principle of operation of a PSFB DC-DC converter and theory regarding PID control is taken from the previous course. In order to understand grounding and charging for shore-connected ships, the remaining content will cover this topic theoretically, as well as a literature review.

2.1 Cold Ironing Galvanic Corrosion Phenomena in the Presence of Leakage Current

The meaning of cold ironing, or shore-to-ship, consists of supplying the ships with the electrical systems existing on shore[13]. Several ports worldwide are equipped with HVSC, and this technology is an increasing technology as it can be utilized in battery charging of hybrid and all-electrical ships. HVSC is a well-developed technology, and even though standards have been followed, there are still challenges with galvanic corrosion on the ship's hull while connected to the shore-side electrical system. Corrosion is an undesired phenomenon since it shortens the ship's lifetime and can be unsafe if a voltage potential arises between two charging ships[1]. Four factors are contributing to the corrosion phenomena [14]:

- Anode- a place where corrosion occurs and current flows from.
- Cathode- pole where no corrosion occurs and current flows into.
- Electrolyte (seawater)- a medium capable of conducting an electric current by ionic current flow. Seawater has high electrical conductivity, with a resistivity of about 0.25-0.2 $\Omega \cdot m$, which depends on salinity and water temperature[15].
- Galvanic or metallic path- a solid, galvanic connection between the anode and the cathode, allowing the current to return and closing the electrical circuit's path.

The corrosion issue arises during shore-to-ship connection when a ship is constructed with a metallic hull (steel, aluminum, uniform materials) and connected to the grounding system on-shore via a low-resistance PE conductor. As a consequence, galvanic corrosion arises since current can flow between the ship's hull and the grounding system on-shore with return through the seawater, as depicted in figure 2. Besides, ships with an aluminum hull will experience more accelerated corrosion than a ship with a steel hull because aluminum is less noble than steel[1].

A critical notification to be taken into account when considering the grounding of ship power systems is that an earthing connection is made on a ship by contact of the hull to the seawater. All electrical systems on a ship are referenced to this ground, or also termed as zero potential reference point[16].
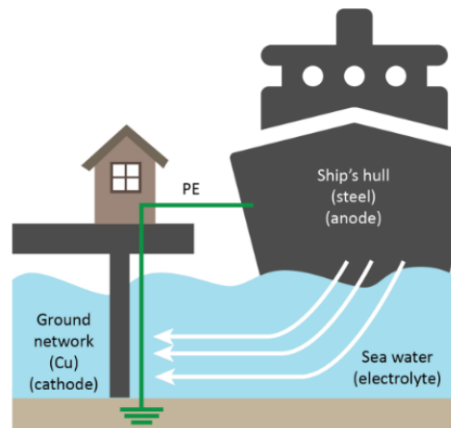
Figure 2: Galvanic corrosion during shore-to-ship connection, illustration SINTEF[1], reprint with permission from Eirill Mehammer

2.1.1 Literature Review Regarding Grounding and Corrosion Issues during Shore-to-Ship Connection

The corrosion issue during cold ironing operation is not a new problem, and several authors have investigated this topic. In [14] highlighted the corrosion issues that arise in an AC-powered MV cold-ironing system with regards to the currents flowing between the ship's hull and steel rebars in the concrete pier. The authors stated that when the cable-to-hull capacitors are asymmetric on the ship-side, leakage current increases between the ship's hull and pier. Consequently, it leads to accelerated corrosion on the ship's hull and the pier.

In [1], SINTEF had been collected measurements of voltages, currents, and galvanic potentials at different quays in Oslo, Larvik, and Kristiansand, which highlighted several issues that must be taken into account if a significant rollout of HVSC systems is to take place. Otherwise, both ships and steel constructions at the quays would suffer from accelerated corrosion, and transferred touch voltages could arise in case of a ground fault. Based on the field measurement, SINTEF recommends a grounding strategy with galvanic separation in the low-resistance PE conductor during power delivery from shore.

This type of grounding system is known as the TN-island system, as seen in figure 3 for cold ironing, and has also been suggested by [13]. The latter reference describes a short outline of a cold ironing system and its usual grounding system. Besides, the paper highlights the importance of avoiding any connection between the grounding system on-shore and the common equipotential node on the ship to reduce leakage current. Therefore, three different technical solutions were introduced and their respective benefits and drawbacks. However, the authors in that paper concluded that the TN-island grounding system was the most beneficial. In [2], illustrates the current TN multiple grounded system (suggested by the standard) was compared to the TN-island grounding system, and the advantages of an island system were highlighted. The paper showed the decrease of the risks for corrosion of the ships and the transfer of touch potentials.
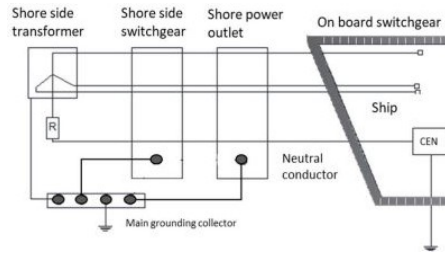
Figure 3: TN-island grounding system[2], with permission from G.Parise

[17] analyzed in detail the different components of HVSC systems for modern ships. Relevant standards were discussed, and the system behavior in the case of single phase-to-ground fault and three-phase short circuits was analyzed. When a single phase-to-ground fault occurs, the value of the NGR on the shore-side TF plays a crucial role, and the operation with earthing switch results in lower values of touch voltage. As a result, the range of NGR values between 125 Ω and 3500 Ω were stated as permissible values without violating reference standards and any operating scenarios. Corrosion issues regarding grounding strategies and standards for HVSC in AC distribution exist on a large scale and have been well-developed throughout the years. This is because the AC-grid is more widely used than DC-powered systems[18].

Studies about shore-to-ship connection with DC distribution on ship-side interconnected with shore-side AC-grid have not been found in the literature. Nevertheless, a general guideline for 1 kV to 35 kV MV DC-powered systems on ships is presented in IEEE Std 1709-2018 [10]. The main purpose of this practice was to provide analytical methods, preferred interconnection interfaces, performance characteristics, and testing for MV DC electrical systems on ships. The paper recommends that all loads are galvanically isolated from the MVDC bus. The IEEE general guide also specifies that if there is no intentional DC path to the ground, there is no DC reference point for the MVDC bus to establish balance. As a consequence, the presence of even a small leakage current in the mA-range can cause unpredictable DC offset. Therefore, the guideline recommends a ground reference point on the DC-side through high-value resistors (in $k\Omega$) to common ground from each DC bus. Several other grounding structures exist for DC-powered distribution, so an overview of the existing grounding structures will be presented further in this paper.

2.2   Shore-Side Transformers

In order to connect a berthed ship to shore-power for cold ironing operation, a dedicated substation TF of adequate rating is required. A step-down TF reduces the voltage from the HV grid into a lower voltage. By open-circuit conditions, the magnetic core loss resistance R_c and the magnetizing reactance X_m can be calculated as follows[19]:

$$\frac{1}{Z_{ex}} = \frac{1}{R_c} + \frac{1}{jX_m} = \frac{I_{oc}\angle\theta}{V_{oc}\angle 0^o} \tag{1}$$

where V_{oc} and I_{oc} is the open-circuit voltage at 0° and no-load current with PF angle, respectively. The PF angle can be calculated as:

$$PF = \frac{P_{oc}}{V_{oc} \cdot I_{oc}} \tag{2}$$

where P_{oc} is no-load losses. The PF angle θ can therefore be stated as:

$$\theta = cos^{-1}(PF) \tag{3}$$

2.3   Grounding Systems in AC and DC Powered Systems

There are three defined and standardized grounding configurations, and they are based on the ground connection types of the source buses and the conductive parts of the system[4].

In Norway, there are mainly two types of grounding systems; 230V IT systems and 230/400V TN systems[20]. The 230 V IT system is the most common in Norway and is used in 70% of the grid. The TN 230/400 V system is utilized in new grid areas, and some former IT systems are rebuilt to TN systems[21]. TT grounding is more common in other countries, such as Belgium, Italy, and France[22].

In DC-powered systems, DC fault currents are critical when the supply voltage is above 50 V_{dc}, and must be considered when designing a DC electrical system[23],[24]. A vital notification is that the DC output filter of the power distribution connected with the rectifier stores a remarkable amount of energy during a short-circuit fault that must be dissipated[25]. Since DC distribution does not have the natural zero-point as a three-phase AC system, the grounding of the DC output must be done in the way of a derived midpoint[26], [23],[24], or by grounding one of the poles.

The grounding configurations are suitable for AC-electrical systems when considering the design and operational requirements. Similar safety and functional purposes also regard DC systems, so most of the strategies are also suggested for DC-powered systems in the literature[27], [28]. Knowing the fundamentals of the existing grounding structures for AC and DC electrical systems is necessary for selecting the most optimal grounding system for its distributed electrical system, and they will be listed further.

An essential notification within grounding configurations is the difference between earthing and grounding. The latter refers to connecting the live part (the part that carries current under normal conditions) to the ground, for example, neutral of the TF. Grounding protects the power system's equipment and provides an effective return path from the current-carrying live part back to the power source. Moreover, the definition of earthing is connecting the dead part (ECP) that might become alive when basic insulation fails. ECP, f.ex frames or mechanical chassis do not carry current during normal conditions. However, earthing works during a fault condition, and an ECP connected to a PE conductor safely drain the ground-fault current to the source[11].

2.3.1   TN-Grounding Systems

A TN-grounding system denotes a connection between earth and the electrical device being supplied, where T has a direct connection of a point to earth, and N has a direct connection to neutral at the origin of installation, that is connected to earth[29]. In DC systems, the neutral point of a converter/rectifier can be derived using two equal-valued capacitors in series. Moreover, advantages of TN-grounding systems include having enough fault current to be detected, which requires low grounding impedance, and limiting fault current by adjusting the ground impedance. However, for HV-applications, the touch voltage is high[30]. In the TN-grounding system, stray voltages (or neutral-to-earth voltage) can appear, even in normal conditions. Although earthed at the substation, the neutral conductor might be energized above ground. Moreover, TN systems have three subclasses; TN-S, TN-C, and TN-C-S, and they will be explained further.

TN-S systems separate N and PE conductors. TN-S grounding systems for AC and DC distribution can be seen in the figures 4(a) and 4(b), respectively. This configuration has higher safety than TN-C since, if the conductor

becomes disconnected, the protective features remain intact[9].
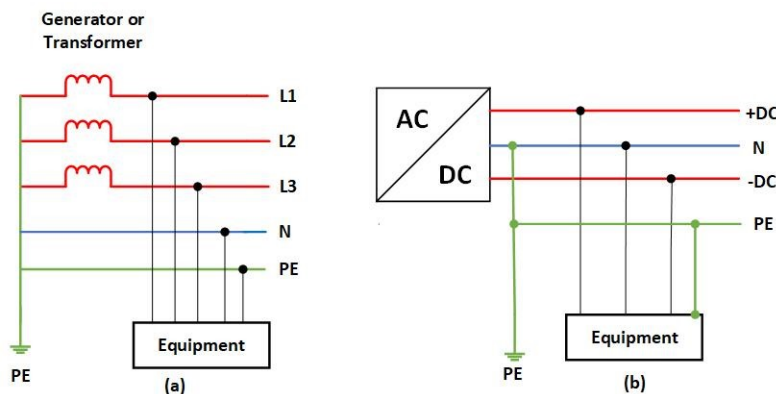
Figure 4: TN-S grounding for (a) AC system and (b) DC system

TN-C systems combine the two conductors to the PEN conductor[9], and the figures of TN-C systems for AC and DC can are shown in the figures 5(a) and 5(b), respectively.
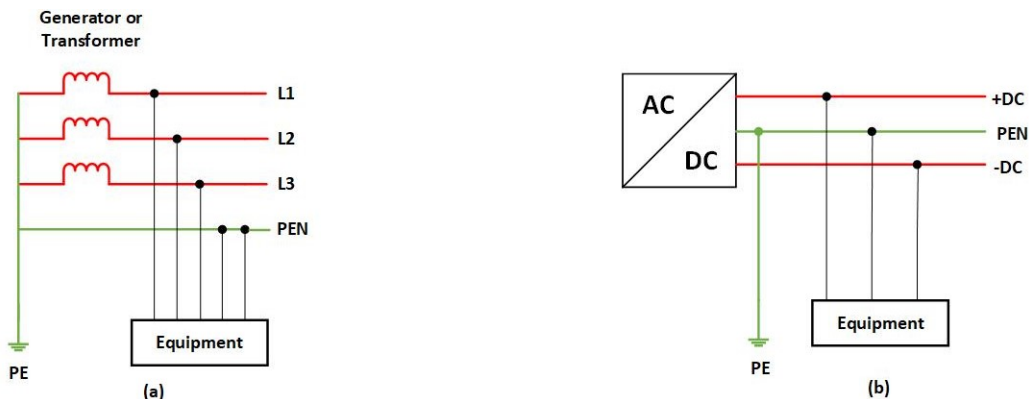
Figure 5: TN-C grounding for (a) AC system and (b) DC system

TN-C-S systems are a combination of TN-S and TN-C systems, where the PEN-conductor is split into a PE-conductor and an N-conductor[21], which can be seen in the figures 6(a) and 6(b) for AC and DC systems, respectively.
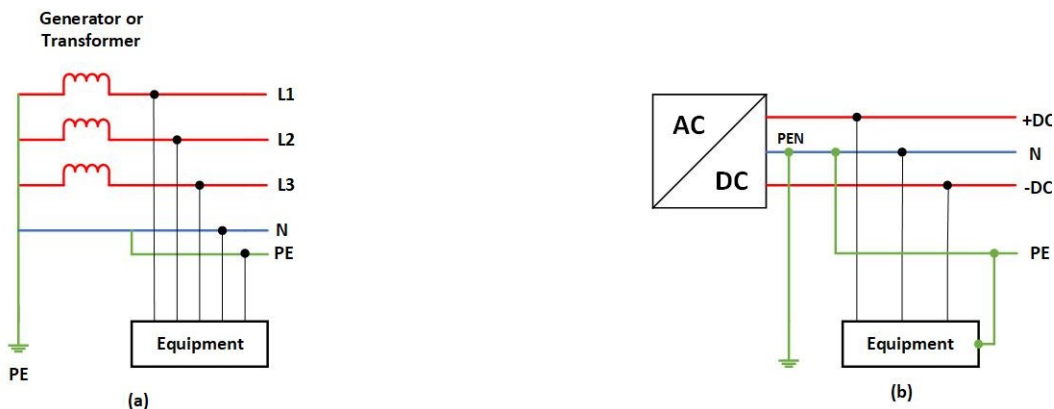
Figure 6: TN-C-S grounding for (a) AC system and (b) DC system

2.3.2 IT Grounding System

In IT-grounding systems, the supply is isolated from earth and is either unearthed or connected to earth through a high impedance connection. The exposed equipment of the electrical system is directly connected to PE, and within this grounding configuration, the supply and the ECP are earthed. Two advantages of the IT-grounding system are that if there is a phase short-circuit, it will go through the TF's neutral point. As a result, there will be a small fault current to the ground due to high impedance, so the protection does not trip[21]. The other advantage is that with an IT-grounding system, it can continue providing energy to the loads[9].

However, disadvantages with IT grounding systems are unpredictable fault current paths through the distributed generations when a second LG fault occurs, and it is challenging to locate the fault current[31]. By the utilization of the IT grounding with a middle point solidly grounded, an IMD can supervise the insulation resistance between the power lines and earth. The IMD can continuously monitor the impedance to ground by injecting both an AC and DC current through the neutral point of the power system. If the impedance decreases below a threshold value due to a first ground fault, a visual alarm will be initiated[11].
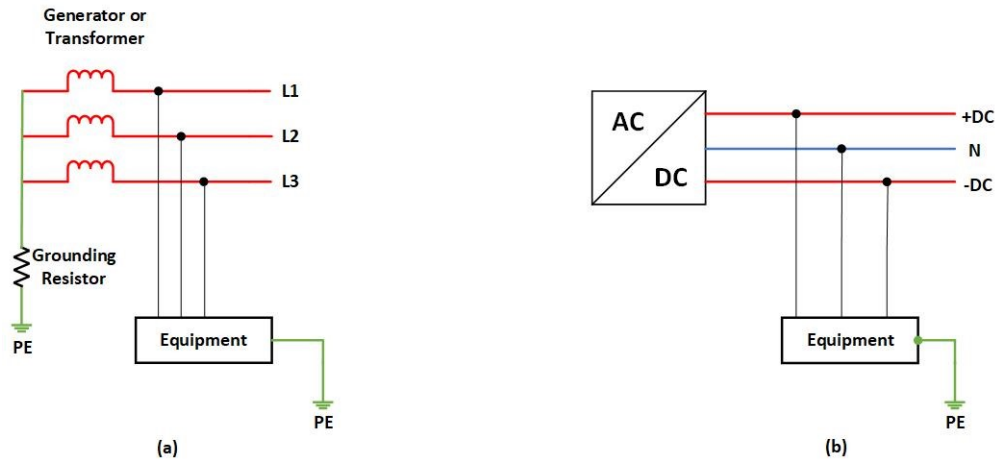
Figure 7: IT grounding for (a) AC system and (b) DC system

2.3.3 TT Grounding System

In a TT-grounded system, the neutral conductor of the TF/generator/converter and PE conductor of loads/equipment are separately connected to the ground point. This type of grounding configuration is very straightforward to install, and the fault will not transfer to other parts of the grid. However, circulation of current and the possibility of high voltage stress are the main drawbacks of this grounding structure[32].
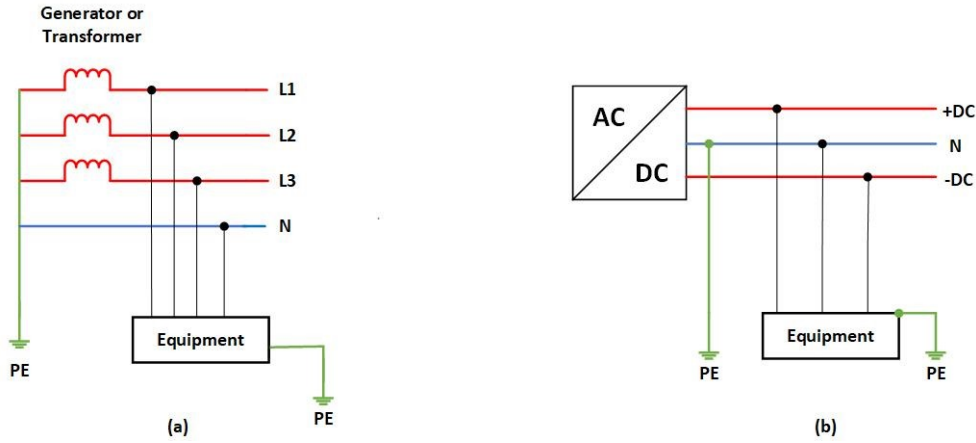
Figure 8: TT grounding for (a) AC system and (b) DC system

2.4 Neutral Grounding Resistor

According to [17], international standards require that the neutral point of the shore-connected TF is equipped with a NGR. A NGR is a resistor used in an AC distribution connected between the TF's neutral point and the ground[14]. According to IEEE 80005-1 standard, the TF is equipped with a NGR on the secondary Y-connected side [17]. NGRs limit the fault current to a safe value for the electrical grid components and prevent any possible mechanical damage due to strong magnetic fields which occur during high short-circuit current flow[14]. The working principle of the NGR can be seen in figure 9. The NGR value must be defined to guarantee the protection and safety of the equipment and personnel in case of a single phase-to-ground fault.

There are two different methods for grounding with a NGR; LRG and HRG. In LRG, the NGR is sized so that the resistive component of the fault current is remarkably higher than the total system charging current, which is termed the current that flows through the parasitic capacitances. HRG implies that when there is a single phase-to-ground fault, the fault current's resistance is higher than the capacitive. Besides, compared to LRG, HRG provides lower damage risk at the fault location[17], but LRG makes the tripping of the protection system easier and implies lower values for transient overvoltages[33]. When a ground fault condition happens, the HRG will limit the phase-to-ground current to a lower level of 25 A[34][35][36]. The NGR is monitored continuously for open or short-circuit conditions, and the CBs open automatically on both sides if any abnormalities are detected[37].

In order to calculate the value of the NGR resistance, it can be termed as:

$$NGR = \frac{U_n}{\sqrt{3} \cdot I_f} \qquad [\Omega] \quad (4)$$

where $\frac{U_n}{\sqrt{3}}$ is the line to neutral voltage, and I_f is the ground fault current rating.
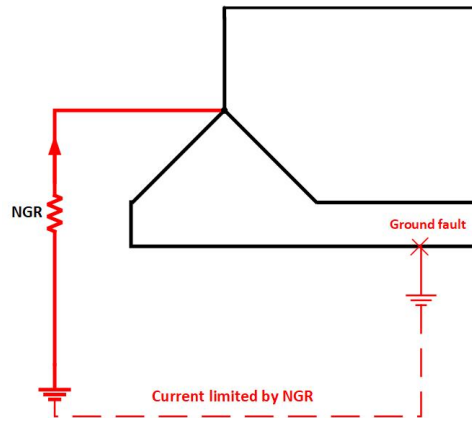
Figure 9: Working principle of a neutral grounding resistor

2.5 Nominal Current Capacity

Cables that supply electrical power have some resistance, and their respective resistances are based on their nominal current capacity and their respective cross-sectional area. So, in order to calculate nominal current, it can be calculated as[38]:

$$I_N = \frac{P_N}{V_N} \qquad [\text{A}] \quad (5)$$

where P_N is the nominal power and V_N is the nominal voltage.

2.6 Faults in AC and DC Distributed Systems

In AC systems, there are mainly three types of phase faults. The first is a single phase-to-ground fault, see figure 10 a), which is the most frequent fault (60-70% of occurrence) and will happen when any one of the lines is in contact with the ground. The next is a phase-to-phase fault, as depicted in figure 10 b), which happens when two lines are short-circuited (5-15 % of occurrence). The third is double phase-to-ground fault (15-25 % of occurrence) and occurs when two lines are short-circuited and are in contact with the ground[39]. See figure 10 c) for an illustration of a double phase-to-ground fault.
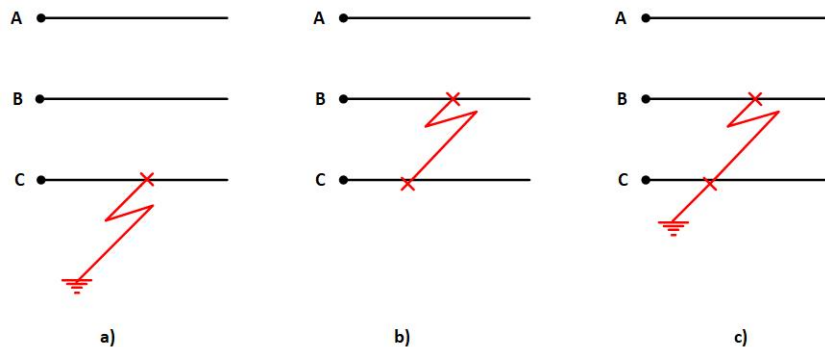
Figure 10: AC system fault types (a) Phase-to-ground, (b) phase-to-phase, and (c) double phase-to-ground

Furthermore, in DC distributed systems, two types of faults can arise on the DC-line, and they are termed LL and LG[4], as depicted in figures 11a) and 11b), respectively. LL fault occurs when a conductive path exists between the positive and negative poles of the system[40], as depicted in figure 11a). During a LL fault, a large current arises, and the current is usually limited by the system resistances[32], [41] and not affected by the chosen grounding

strategy[4]. LL faults are less common than LG faults, but they are potentially more dangerous than LG faults and can be more difficult to detect[40].

In DC-distributed systems, a LG fault is more common and is directly affected by the chosen grounding system. The LG fault reduces the voltage of the faulted conductor to almost zero and, depending on the grounding structure, may increase the voltage of the un-faulted line. The LG fault puts, therefore, the personnel/equipment safety at risk[32], [41]. Hence, detecting LG faults and managing the associated overcurrent and overvoltage stresses are among the high-priority objectives of DC-distributed grounding strategies[4].
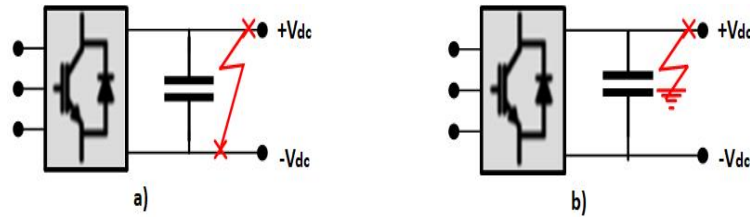
Figure 11: DC system fault types (a) LL and (b) LG

The ground fault can be divided into three categories, which depend on the period the ground fault occurs, and they will be explained further.

2.6.1 Constant Ground Fault

A constant ground fault is the most common ground fault[42], and the ground fault is continuously[43]. In addition, it is the most accessible ground fault to detect and locate[42]. When this type of ground fault occurs, it stays at the same level, or it increases[43].

2.6.2 Intermittent Ground Fault

In an intermittent ground fault, it comes in and out with relatively long periods, in more than 5 minutes, in either a fixed or random off-period. An intermittent ground fault can be more challenging to detect since it is periodical; however, it can be found with standard ground fault detection equipment[43].

2.6.3 Transient Ground Fault

A transient ground fault can usually not be found with standard ground fault detection equipment. Moreover, this fault category can be divided into two sub-categories, termed "pulses" and "spikes ."The former has a short duration (0.5 to 5 minutes) with either a fixed or random off-period. The latter has a shorter period than spikes (0.01 to 5 minutes) duration with either fixed or random off-period[43].

2.7 DC Fault Isolation

DC fault isolation is necessary to stop the high short-circuit fault flow in the system by disconnecting the faulted part from the healthy one. When a fault detection and location are completed, the next step is fault isolation to maintain the system's reliability and stability, which is essentially important where a common DC bus is employed such that the whole system is not interrupted by a fault. DC fault isolation can be obtained with DCCBs or

without CBs. Without DCCBs, isolated power converters, fault-tolerant generators, or the variant 2L-VSC can be utilized. Existing DCCBs are fuses, DCCBs, hybrid CB, and mechanical CB[44]. As a comment, only isolated DC-DC converters will be contemplated in this paper.

2.8 Overview of Existing Grounding Devices in DC Electrical Systems

A comprehensive investigation regarding technical characteristics of different grounding strategies is presented for DC traction [27], [45], [46], DC shipboard, [10], [8] and HVDC transmission [47], [48] systems. DC MG grounding is investigated in the papers [49], [50], [32], [51], [52], [53], [40], [41]. However, as a comment, they do not provide comparison between different grounding strategies in order to find the most optimal grounding strategy that suits for its respective electrical system. Moreover, studies on impacts of grounding configurations on DC MG fault response are proposed in [49], [50], [32], [51], [52]. The main drawback with these papers is that they do not investigate the impacts of different grounding devices which is very important for choosing the most suitable grounding system. Reconfigurable grounding strategies, i.e., diode and thyristor grounding, are discussed in [41], concerning their benefits and drawbacks.

In [53], impacts of DC systems grounding strategies on personnel safety are investigated. HR grounding strategy is proposed in [40] in order to enable ground fault ride-through capability in DC MGs. These studies do not involve comprehensive information to enable appropriate grounding system design for a DC-powered system. In [4] investigates and compares different DC MG grounding strategies that involve the choice of grounding configurations and grounding devices. In [9] proposed a comprehensive review regarding DC MG protection which includes DC fault current characteristics, ground systems, and fault detection methods.

Grounding devices of DC electrical systems can be shared into four groups as follows[30], [9], [4]:

- Ungrounded system,
- Solidly grounded system,
- Resistive grounded system, and
- Reconfigurable grounding systems.

2.8.1 Ungrounded DC Systems

In ungrounded DC systems (see figure 12), neither the mid-point of the DC-link nor poles are not intentionally connected to any grounded system. Since this grounding structure does not need any grounding device to be connected to the ground, it will be simple to implement[30]. However, an ungrounded DC system provides no path for the flow of stray current. This grounding strategy is, therefore, the best choice for applications with high susceptibility to corrosion, such as DC traction systems[27], [9]. Nevertheless, suppression of leakage current with an ungrounded DC strategy may result in safety concerns for personnel[4].

LG fault causes the voltage of the faulted conductor to drop to zero immediately. It forces the voltage of the faulted conductor to rise to about 2 per unit in steady-state and causes zero steady-state fault current. However, discharge of the faulted cable stray capacitances and their interaction with the system inductances lead to transient oscillations with limited magnitudes and duration. An essential concern related to the ungrounded system is the LG overvoltage on the un-faulted conductor. Besides, the DC grid can continue to operate under LG faults, as the

LL voltage is not affected by the fault[4].
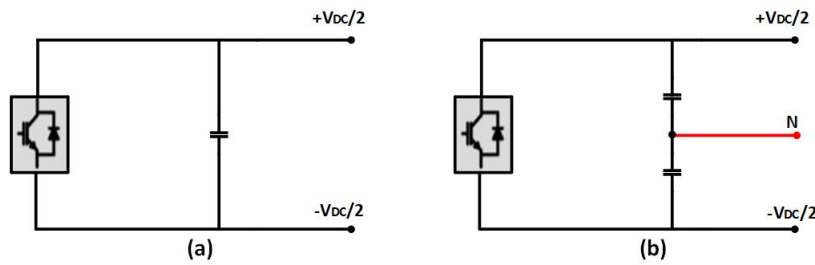
Figure 12: Ungrounded DC system, (a) unipolar system, and (b) bipolar system

2.8.2 Solidly Grounded DC Systems

In DC-distributed systems, the term grounded is referred to a system where at least one conductor or a point (usually the mid-point of the DC-link or one of the positive or negative poles of the DC grid) is intentionally grounded[26], [30]. Solidly grounded DC systems were a standard grounding mode of power distributing shipboard systems in the earlier period[8]. In this type of grounding structure, there are two options regarding the point of connection to the ground, as shown in figure 13. The negative or positive pole of the unipolar DC-system and the middle-point of the bipolar DC-system can be solidly (directly) connected to ground[30], [27], [4]. However, in a unipolar structure, only one level of voltage ($+V_{DC}$) is available[9]. The simplicity of implementation and cost-effectiveness turn this scheme into a popular choice for grounding DC-grids[5].

With this grounding structure, extreme corrosion is one of the main challenges[30], [27]. The requirement of costly insulations for the prevention of corrosion has made it an unsuitable choice for grounding the applications with high susceptibility to corrosion[9], [4]. In a unipolar solidly grounded structure, the negative polarity conductor is grounded, so the LG fault causes the LL voltage to drop to zero and thus causes service interruption. In addition, the solid grounding provides a path for the large discharge current of the stray cable capacitances and the converter DC-link capacitors[4].
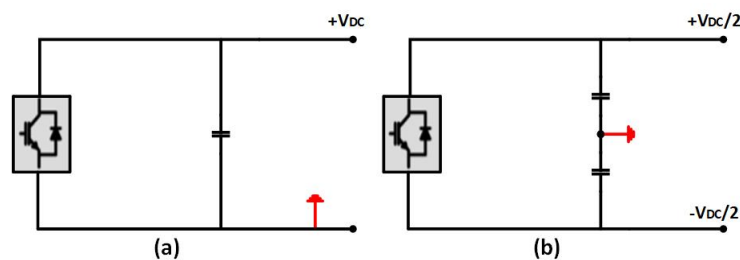
Figure 13: Solidly grounded DC system, (a) unipolar system, and (b) bipolar system

2.8.3 Resistive Grounded DC Systems

Figure 14 indicated the grounding system by utilizing a resistor (R_G) on its structure. As shown in figure 14(b), the middle-point of the DC-link or one of the positive or negative poles can be connected to the ground through a grounding resistor[27], [4]. The main reason for utilizing resistive grounding schemes is to improve the resilience of DC-systems during severe faults[9]. Depending on requirements, the resistor would be chosen low or high. In general, the selection of a suitable grounding resistor is the leverage of achieving an optimized response for both

regular and faulty conditions[30], [27], [9].

Figure 15 shows another resistive grounding strategy that is called parallel resistance grounding and can be utilized for both unipolar and bipolar DC systems[30], [4]. Based on the figure, two equal-valued series resistors are connected to the poles, and the middle-point of these resistors is solidly connected to the ground[54], [47], [55].

The utilization of a grounding resistor reduces the leakage current amplitude and its corrosion effects[4], [56]. The intensity of the corrosion depends on the value of the resistor. A LR grounding resistor slightly attenuates the leakage current, while a HR value can block the leakage current and its corrosion effect[30], [9], [4]. Besides, a low grounding resistor and consequently a high rate of leakage current imposes a considerable power loss to the DC system[5].

When the faulted conductor is discharged to 0 V in a unipolar LR-grounded system, the discharge current is drastically limited by the grounding resistor. Even though the larger grounding resistor effectively limits the discharge current, it causes larger overvoltage on the un-faulted conductor and slower decay of the transient fault current. Therefore, choosing the appropriate grounding resistance involves a compromise between the overcurrent and overvoltage stresses[4].

For unipolar HR-grounded systems, this structure experiences a very fast transient response. On the other hand, if a fault occurs on the positive pole, the other pole is forced to jump 2 per unit. Therefore, the insulation must be large enough to tolerate full DC voltage. This grounding structure does not suffer from power dissipation in which the power loss can be less than 0.01% of the nominal power[5]. Therefore, the power system can be maintained continuously with an insignificant disturbance. The reason for the low power dissipation is that only parasitic capacitance will discharge, and they will have little energy stored, which makes the fault current hard to notice[57]. The main drawback with the HR grounding system during a LG fault is that the power system does not draw enough current to trigger a CB or fuse operation, which makes the fault difficult to localize[58].
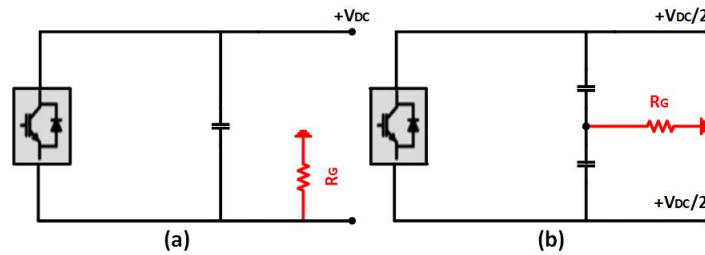
Figure 14: Resistive grounded DC system, (a) unipolar system, and (b) bipolar system
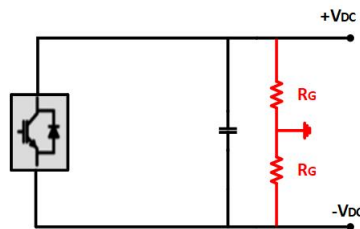
Figure 15: Unipolar parallel resistor grounded DC system

2.8.4 Reconfigurable Grounded DC Systems

A reconfigurable grounding system provides the opportunity to work in a wide operating area from the ungrounded mode to the solidly grounded mode[30], [27], [4]. In normal conditions, this system is ungrounded, while it turns to the grounded system under abnormal ground fault conditions. Then, using this structure, the benefits of both grounding systems can be obtained during normal and fault conditions. A diode grounded DC system can be seen in figure 16 a). Conducting the diode will reconfigure the structure from ungrounded to the grounded mode.

Determination of the conduction threshold in diode grounded mode depends on the requirements of applications which is performed by utilization of a series number of diodes connected to the negative pole[30], [9]. When a LG fault arises in a diode-grounded structure, the system behaves like a solidly grounded system. Therefore, its fault response is similar to a solidly grounded DC-powered system. The only difference is in the ON-state resistance of the diode, causing a small transient voltage on the negative conductor when the current passes through the diode[4].

As depicted in figure 16 b), there is another reconfigurable grounding strategy that utilizes a thyristor on its grounding structure [30], [27], [9]. The main reason behind the utilization of a thyristor is actively controlling the structure of the DC system. The thyristor actively reconfigures the grounding system from the ungrounded mode to the solidly grounded mode. This reconfiguration arises when the voltage or current of the thyristor exceeds a threshold value[27]. Limitation of leakage current is one of the motivations behind proposing the idea of reconfiguring grounding strategy. In the normal operation, the system is in the ungrounded state where the flowed current to the negative pole (leakage current) is negligible[4]. Therefore, the issue of leakage current corrosion during normal conditions is effectively solved. Under a fault condition, the voltage of the negative pole exceeds the threshold value (60 V for the operator's safety considerations), and consequently, the diode/thyristor conducts. Then, the grounding structure switches to the solidly grounded mode upon exceeding the voltage threshold during a fault condition[4].

If a LG fault occurs in a thyristor-grounded DC system, almost the same will happen as in a diode-grounded system. The thyristor turns ON when the fault is detected. The thyristor in the ON-state is electrically equivalent to a diode with a similar ON-state resistance[4].
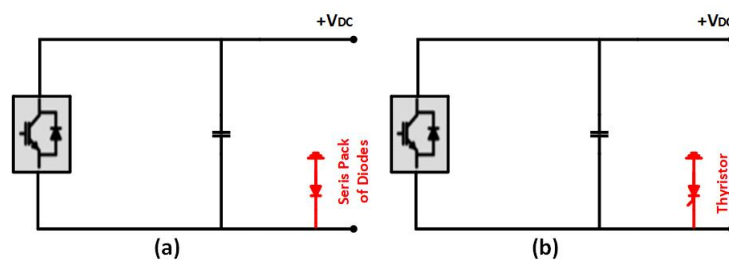
Figure 16: Reconfigurable grounded DC system, (a) diode grounded, and (b) thyristor grounded

2.9 Impacts on DC grounding

Several factors have an impact on the chosen grounding system, such as the following: CMV, leakage current, fault ride-through capability, DC fault detection, and LG fault response [59],[26], [30]. These factors are simultaneously conflicting with each other so that an optimized factor will lead to a mal-operation of another criteria[5].

2.9.1 Leakage Current

Leakage current (or stray current) referrs to current that flows from the main to the ground[60] due to a deficiency of isolation[61]. The current leaks from the grounded point to the ground, and, consequently, corrosion arises at the locations the leakage current leaves the conductor for an extended period of time[61]. Leakage current can appear if the insulation of the electrical wires deteriorates due to dielectric contamination, excessive overloads, excessive voltage stress due to overvoltage, and aging. Overvoltages cause abnormal stress within the insulation, leading to cracking or delamination of the insulation. The insulation failure while in service can cause significant damage to equipment and the equipment connected to the system. Insulation failure can cause dangerous voltage, fire, high fault current and explosion, damage to equipment and property, personnel injury, and fatal accident[62],[11].

Moreover, the magnitude of the leakage current depends highly on the resistance of the flowing path. Implementing a resistor in this path considerably attenuates the magnitude of the leakage current and limits its harmful corrosion effects. When the ground-fault current path of the electrical system is effectively designed, fuses, CBs, and ground-fault detectors are allowed to open appropriately when ground-fault conditions arise in the electrical system. From the standard for personal safety, ground fault circuit interrupters are activated when the leakage current exceeds 30 mA[11], [63].

2.9.2 Common-Mode Voltage

The CMV refers to the average potential level between conductors and the ground. This voltage oscillates with HF components which causes the excitation of parasitic capacitances and consequently leads to the flowing of CM currents through the body of equipment[64]. Hence, the fluctuation of CMV threatens equipment operation as well as personnel safety if it exceeds a certain standard threshold value[27], [51]. The primary solution is to control the level of CMV, which is tied to the selection of a proper grounding structure[5].

2.9.3 Fault Ride-Through Capability

Fault-ride-through capability refers to the electrical system's ability to continue during a single LG fault[8]. This feature is highly demanded in critical applications, such as data centers, navy, and shipboard. However, the fault ride-through capability can be adverse for ships during shore-to-ship connection. The electricity outages in the mentioned applications cause high financial forfeiture, stability concerns, or even security consequences. Owing to the corresponding affection of grounding systems on this criterion, the ability to ride through the faults is accessible by selecting a suitable grounding scheme[54].

2.9.4 DC Fault Detection

Adequate protection in an electrical system is significantly tied to the accuracy and speed of the fault detection[65]. In DC-powered systems, the line impedance is much lower than that of AC systems, and the fault current would rise to hundreds of amps during a relatively short period. Hence, the detection and clearance of faults in a fast and precise manner is necessary for DC distributed systems[45], [66], [67]. Furthermore, the DC faults are not easily detectable in every grounding structure, and the implemented method must be compatible with the utilized grounding system. Concerning the dependency of fault detection on the grounding systems, these systems can be considered as an option to relieve the procedure of fault identification in DC-powered systems[5].

There are several fault detection methods, and one of them is signal processing-based methods. Signal processing technique methods are based on analyzing the output signals. They do not involve an explicit input-output model of the target system, and the output features correlate with the system faults. Typical signal methods include FFT, spectrum estimation, and the WT. Another fault detection method is advanced strategies, including AI and ML-based approaches. When a fault occurs in the power system, it creates a massive current that could affect the entire system operation and shuts down the whole system. Furthermore, another fault detection strategy is model-based fault detection and identification, which incorporates a detection factor as well[44].

2.9.5 Line-to-Ground Fault Response

In DC-powered systems, when a fault occurs, overvoltage and overcurrent spikes are the most harmful phenomena. Therefore, it is essential to protect the equipment and sensitive loads against destructive overvoltage/current spikes under fault conditions. Various grounding schemes provide different behavior for the voltage and current of the faulted branch[68].

Based on the impact factors mentioned above, DC electrical systems' reliability and safety requirements are conflicting issues affected by the mentioned functional characteristics. The behavior of the characteristics in terms of safety of equipment and personnel, minimum corrosion in the surrounded infrastructures, detectability of DC faults, fault ride-through capability, and non-concerning fault responses assure the optimal performance of a DC electrical system that varies under different grounding system[5]. Therefore, proper selection and designing of a grounding system require a comprehensive inspection of the mentioned aspects. Table 1 compares the existing grounding devices with essential factors for impacts on DC grounding.

Table 1: Comparison of Existing Grounding Strategies for Impacts on DC Grounding[4][5]

Grounding Strategy	Ungrounded	HR Grounded	LR Grounded	Thyristor Grounded	Diode Grounded	Solid Grounded
CMV	High	High	Low	Moderate/ High	Moderate/ Low	Low
Transient Overvoltage	High	High	Moderate	Moderate	Moderate	Low
LG Fault Current	Low	Low	Moderate	Moderate/ Low	Moderate/ High	High
Leakage Current	Low	Moderate	Moderate	Moderate/ Low	Moderate/ High	High
Relay Protection	Difficult	Easy	Easy	Easy	Easy	Easy
Service Continuity	Yes	Yes	Yes	No	No	No
System Reliability	Low	High	High	High	High	Low
Insulation Level	High	High	Low	Moderate/ High	Moderate/ Low	Low
Safety	Low	High	High	Moderate/ Low	Moderate/ High	High
Grounding Loss of Power	No	No	Moderate	No	No	No

2.10 Three-Phase Rectifiers

The interaction between the utility supply and power electronic systems depends on the front ends, where line-frequency AC is converted to DC. The front-end of power electronic systems can be classified into three categories[38]:

- Switch-mode converters, where the power flow can reverse in the opposite direction, and the line current are sinusoidal at the unity power factor.
- Thyristor converters, where the power flow can be created bidirectional.
- Diode-bridge rectifiers, where the power flows in only one direction. This rectifier will be explained further.

2.10.1 Literature Review of Three-Phase Rectifiers

In [69] proposed a new mathematical model and control of a 140 kW three-phase AC/DC VSC in the stationary and synchronous reference frames. In general, VSCs enable the provision of constant DC bus voltage. The mathematical model analyzed voltage and current control loops for the VSC[69]. [70] proposed an active PF correction technique for three-phase front-end diode rectifiers. An additional single switch boost chopper was implemented in the proposed electrical circuit. The rectifier was obtained to draw sinusoidal AC current from the source with unity

PF (PF = 1). However, the main drawback with the proposed rectifier was an increase in switching stresses of the switching devices compared to the conventional AC/DC rectifier.

In [3], a single switch three-phase AC/DC rectifier with reduced voltage stress and current THD was proposed, as depicted in figure 17. The reduction of voltage stress on the active switch and the diodes were obtained by integrating a coupled inductor and two buffering capacitors. As a result, the switching loss on the main switch was reduced. Features of a three-phase single-switch boost PF correction converters are a zero-current turn-on for the switch and no reverse recovery in the diode. However, the input PF is relatively low when the duty cycle is constant in the whole cycle line. Therefore, [71] analyzed the principle of operation of a three-phase single-switch DCM boost power factor correction converter. The expressions of the input current and PF were derived and based on them, a variable duty cycle control was proposed.

[72] investigated the operation characteristic of a three-phase uncontrolled rectifier for charging vehicles with passive PF correction. A measurement-based method for estimating the equivalent circuit parameters was achieved. The proposed method can estimate the parameters by the measurements taken under different voltage conditions. In [73], a method for calculation of the current harmonic amplification effect of the charging station based on an investigation of the coupling relationship between current and harmonics voltage of EV charging stations, as well as the definition of the total amplification factor, was proposed. The method's main advantage was that the harmonic amplification effect caused by the active power filters was quantified analytically and accurately during different operation modes of the EV charger. [74] proposed a detection method for open-circuit faults in a three-phase uncontrolled rectifier. The algorithm is based on fault signatures within the output voltage ripple of the rectifier. A demonstration of seven different classes of open-circuit faults can be detected and isolated.
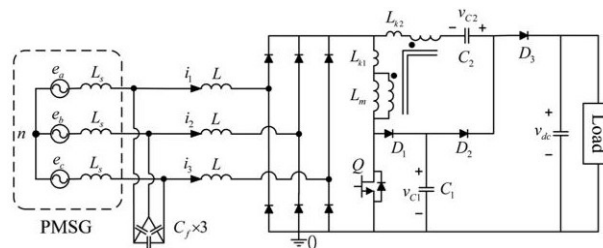
Figure 17: Proposed single swith three phase AC/DC rectifier[3], with permission from Y.L Juan

Figure 18 illustrates a three-phase diode bridge rectifier with a DC-bus capacitor operating as a filter. Diode-bridge rectifiers have been used in many power electronic systems, even though they draw currents with highly distorted waveforms. Diode rectifiers rectify AC to DC across the DC-bus capacitor without control over the DC-bus voltage[38]. A rectifier without a filter will produce pulses at the output. Reduction of these fluctuations can be made if some of the energy is stored in a capacitor while the rectifier is producing pulses and is allowed to discharge from the capacitor between the pulsations[75]. The resistor can be an actual resistive load at the DC-side, the inverter of a variable speed drive, or as a DC-DC converter in reality[76].

2.10.2 Principle of Operation of Three-Phase Diode Bridge Rectifier

With diode bridge rectifiers, the power can only flow in one direction, creating them to operate unidirectionally. The diode bridge contains a top group (D_1, D_3, and D_5) and a bottom group (D_2, D_4, and D_6) of diodes. The group at

the top has its cathodes connected. Therefore, the diode connected to the most positive voltage will conduct, and the other two will be reverse biased. The diode group at the bottom has its anodes connected. Therefore, the diode connected to the most negative voltage will conduct, and the other two diodes will be reverse biased[38]. From each group, at least one diode must conduct to facilitate the flow of i_{dr}, which is the DC-side current. The rectifier has six different diode conduction modes, and they are stated as D_1D_2, D_2D_3, D_3D_4, D_4D_5, D_5D_6, and D_6D_1. Each of the conduction modes last in a time period of $\omega t = \pi/3$ rad, and each diode conducts at an angle of $120°$.
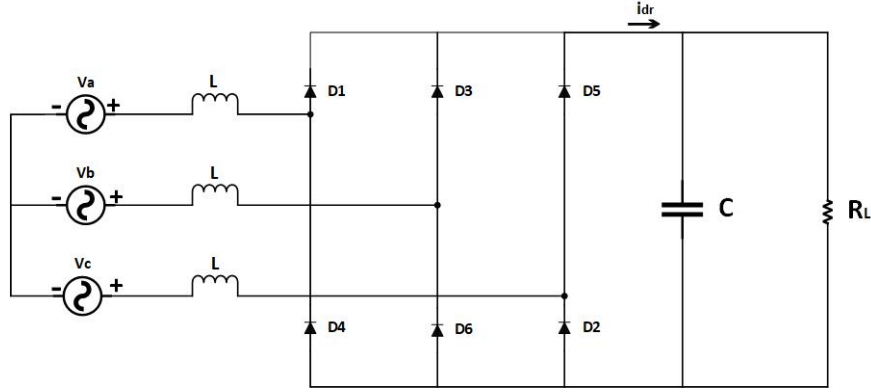
Figure 18: The conventional three-phase diode bridge rectifier

Table 2 shows voltages across the different diodes and the output voltage at each of the different conduction modes. The interval time when a specific conduction mode will be activated can be determined with this table. For instance, D_1D_2 conduction mode occurs when the voltage across all other diodes (v_{ba}, v_{ca}, and v_{cb} are negative. With this, D_1D_2 conducts in the time interval $0 < \omega t < \pi/3$, as depticted in figure 19. The diodes are numbered as in the middle of the figure such that the conduction sequence is D_1 - D_2 - D_3 - D_4 - D_5 - D_6 - D_1, etc. When a diode stops to conduct, its current is commutated to another diode in the same group (top or bottom). Within this way, the sequence of conduction mode can be stated as D_1D_2 - D_2D_3 - D_3D_4 - D_4D_5 - D_5D_6 - D_6D_1 - D_1D_2, etc[38]. The diode rectification results in a DC output voltage with a ripple output, as it can be seen in the bottom of the figure.

Table 2: Voltage Across the Diodes

Device /Mode	V_{D1}	V_{D2}	V_{D3}	V_{D4}	V_{D5}	V_{D6}	V_o
D1D2	0	0	v_{ba}	v_{ca}	v_{ca}	v_{cb}	v_{ac}
D2D3	v_{ab}	0	0	v_{ca}	v_{cb}	v_{cb}	v_{bc}
D3D4	v_{ab}	v_{ac}	0	0	v_{cb}	v_{ab}	v_{ba}
D4D5	v_{ac}	v_{ac}	v_{bc}	0	0	v_{ab}	v_{ca}
D5D6	v_{ac}	v_{bc}	v_{bc}	v_{ba}	0	0	v_{cb}
D6D1	0	v_{bc}	v_{ba}	v_{ba}	v_{ca}	0	v_{ab}
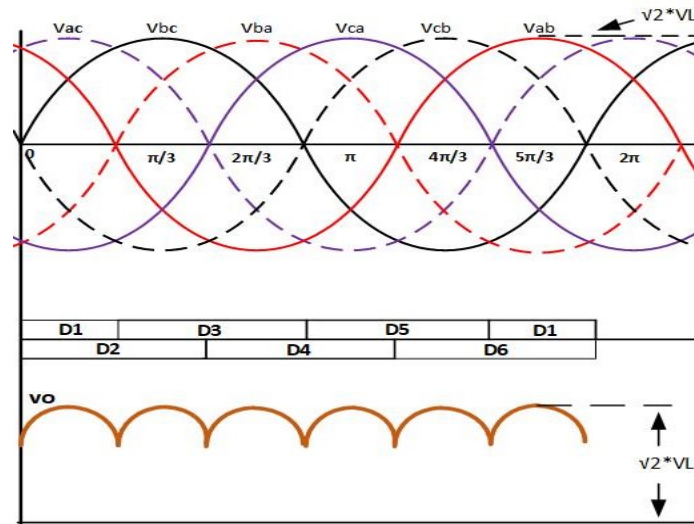
Figure 19: Three-phase diode bridge rectifier waveforms

2.11 Isolated DC-DC Converters

In isolated converters, a HF TF is typically utilized for galvanic isolation of an electrical circuit. Such a converter is necessary for applications where the output must be completely isolated from the input. Galvanic isolation is essential in order to provide safety, flexibility, and for grounding purposes of an electrical system[77], [78]. The types of isolated converters are many, such as half-bridge, full-bridge, flyback, forward, and push-pull converters[79].

Half-bridge power converters are equipped with two main power switches and one multiple-output HF TF[80]. Compared to full-bridge converters, they are normally used in slightly lower power applications[38]. The reason that they are more often used in low power applications is that they must handle currents that are twice as large as for a full-bridge electrical circuit[81].

Among all DC-DC converters, flyback converters are used widely in low power applications[82],[83] because of their low component count, simplicity, and less control complexity[84]. Flyback converters are used to transform DC power supply in the range of a few Watts to 150 Watts[83]. Besides, flyback converters are constructed based on the buck-boost converter. Even though the two-winding magnetic device is presented with the same symbol as a TF, a more "correctly" name for this purpose is "two-winding inductors." Sometimes, this device is also called a flyback TF. Unlike an ideal TF, the current does not flow simultaneously in both windings of the flyback converter. The usual configuration of a flyback converter can be seen in figure 20. The MOSFET switch is connected to the primary side. In order to obtain a positive output voltage, the TF's polarity marks are reversed. A 1:n turns ratio is introduced, allowing for a better converter optimization[81].
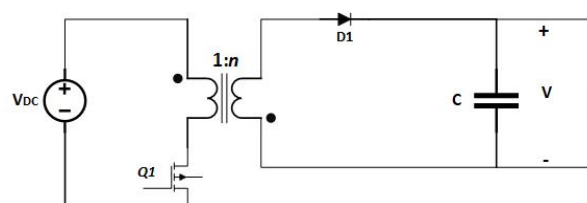
Figure 20: Flyback converter with 1:n turns ratio and positive output voltage

The conventional forward converter can be seen in figure 21, and is based on the buck converter. This converter requires only one switch and is used in applications at low power levels- lower than half-bridge configurations. The output current is non-pulsating, making this converter suitable for applications with high output currents. The maximum duty cycle for the switch is limited to less than 0.5[81].
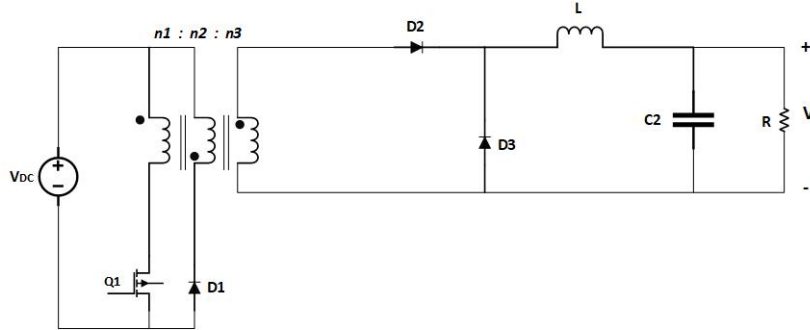
Figure 21: Conventional forward converter

Next, the full-bridge topology is suitable for HV operation, and if equipped with SiC devices, the converter can operate with high switching frequencies[85]. SiC is a wide bandgap semiconductor with several benefits over Si technology. Compared to a Si device, the active area of SiC with the same current rating can be reduced, which decreases the capacitance and promotes operation at higher switching frequencies[86]. The impact of SiC devices across various converter topologies has been studied and was found to be significant for MV (0.4-5kV) isolated DC-DC converters[87].

DAB converter is a topology of a FB converter. They have attracted attention for battery charging/discharging, which needs a bidirectional DC-DC converter, and a DAB converter is, therefore, a suitable solution[88]. These converters can convert power at high frequencies through a two-stage DC/AC and AC/DC structure. A typical/conventional topology of a DAB converter is depicted in figure 22. This type of converter contains a HF TF with a voltage ratio of $1 : n$, and leakage inductance to interface the power transferring between the primary side and secondary side of the HF TF[89]. Besides, the converter is implemented with active full bridges on the primary and secondary sides of the TF[90]. Furthermore, FB DC-DC converter that only needs control on the left side of the converter is the PSFB converter, and will be further described.
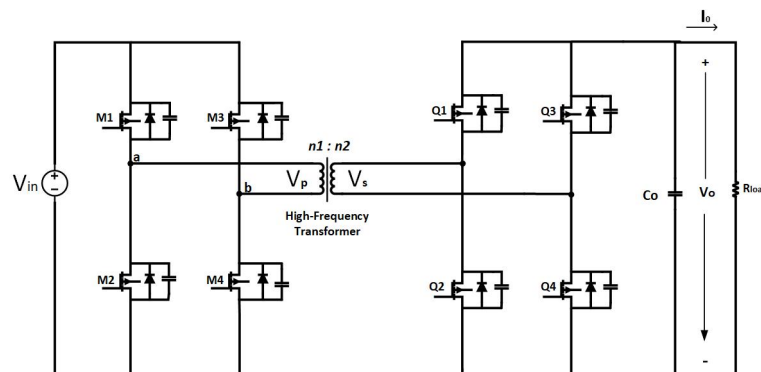
Figure 22: Conventional DAB converter

2.12 Phase-Shifted Full-Bridge DC-DC Converter

2.12.1 Literature Review of Phase-Shifted Full-Bridge DC-DC Converters

The authors of the paper [91] presented a steady-state analysis with a complete characterization of a HV high power full-bridge ZVS PWM converter to establish design equations. An analysis of critical design considerations was also analyzed. The most significant with this paper is that it describes in detail the different stages that must be followed such that ZVS can be obtained.

In [92] presented a 5 kW PSFB ZVS PWM converter, which adopted two clamping diodes on the primary side of the HF TF in order to reduce the parasitic oscillation. In [93] proposed a new PSFB converter with a voltage-doubler-type rectifier for a high-efficiency plasma display panels sustaining power module. The converter did not contain an output inductor, which enabled a simpler structure, lower cost, and lighter weight. Besides, the voltage across the rectifier diodes was effectively clamped to the output voltage. For EV battery charger applications, a 3.3 kW prototype of a PSFB with a new center-tapped clamp circuit was proposed in [94] to obtain high efficiency and reduced output filter. The new center-tapped clamp circuit is composed of two diodes and a capacitor connected to the center tap of the secondary side of the TF. The authors in [95] presented a ZVS full-bridge DC-DC converter prototype for PHEV battery charging applications. The paper presented the detailed operation, design, and performance characteristics. The designed prototype obtained a high efficiency of 96 % such that the charger size can be minimized and the charging time and the amount of cost of electricity drawn from the utility grid.

Furthermore, [96] presented a PSFB series resonant converter for wide load variations, which featured two-mode operation, and at normal loads, the converter operated in series resonant mode. The fixed-frequency phase-shift PWM was utilized at light loads to adjust the effective duty cycle and regulate the output voltage. In order to evaluate the power losses and efficiency of a PSFB converter as a function of the switching frequency, [97] designed a 50 kW PSFB based on theoretical calculations. The converter's efficiency was 99% and 97.5% at full load conditions for 25 kHz and 50 kHz, respectively. [98] proposed a pulse-frequency modulated full-bridge DC-DC converter with a series boost capacitor. The output voltage can be controlled by varying the voltage across the series boost capacitor according to the switching frequency. The converter achieved lower conduction losses compared to a conventional ZVS PSFB converter since the free-wheeling current was eliminated since there was no free-wheeling interval due to a 50% fixed duty operation.

In [99] proposed a 1.2 kW ZVS PSFB converter with the utilization of a separated primary winding technique in order to integrate an additional leakage inductor and TF. The leakage inductance was designed for the ZVS operation of the proposed converter by setting the outer turn ratio. The converter reached lower losses since an additional leakage inductor was built in the TF without an extra magnetic component. In [100] presented a new control methodology that incorporated a variable switching frequency operation at different load power levels. Besides, a design of a state-feedback-based control method was proposed in order to regulate the PSFB converter at variable load and input voltage conditions with the elimination of a load current sensor. The target of ZVS was achieved at all power levels with only utilization of the TF's leakage inductance and removing any additional primary inductor.

2.12.2 Principle of Operation for a Phase-Shifted Full-Bridge DC-DC Converter

Generally, the FB converter is the topology of choice when high-powered converters are required. The FB converter contains four switches, for instant MOSFETs, and they are arranged in an "H" configuration, as depicted in figure 23. This type of isolated DC-DC converter for high-powered converters is a preferred topology due to LV and current stress on the MOSFETs while maximizing the utilization of the TF's capability. The voltage stress across each MOSFETs is the same as the input voltage. The traditional FB converter operates by alternately switching on the diagonally opposite pairs of MOSFET to transfer power from the input to the output through the TF. During the period where all MOSFETs are switched OFF, the current will continue to circulate in the TF's secondary until excitation in the opposite direction by the second diagonal pair of MOSFETs[101]. The output power of the PSFB converter varies with a phase-shift between the duty cycles of two diagonally switches in the right leg and the left leg of the primary side of the converter[100].
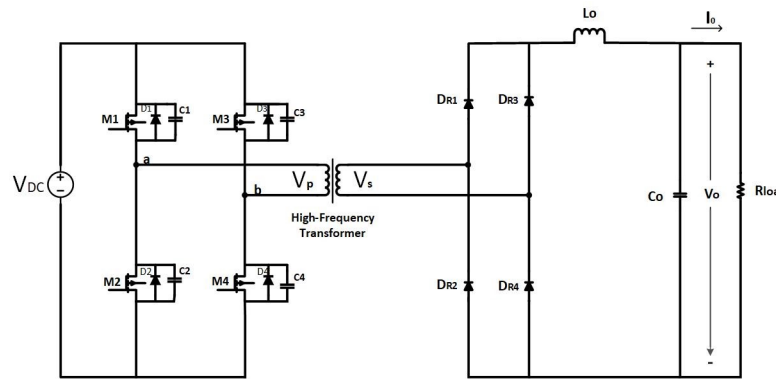
Figure 23: Conventional PSFB DC-DC Converter

As seen in figure 23, the four MOSFET switches form the full-brigde on the primary side of the TF. The MOSFETs contain parasitic capacitance and body diodes, and they can be connected across the switches. The parasitic capacitances are termed C1, C2, C3, and C4, and the body diodes D1, D2, D3, and D4 for their respective switches M1, M2, M3, and M4. The switches M1 and M2 are switched at 50 % duty ratio and 180 degrees out of phase with each other. In the same way, the switches M3 and M4 are switched at 50 % and 180 degrees out of phase with each other. The PWM switching signals for leg M3-M4 of the FB are phase-shifted to leg M1-M2. The amount of the phase shift decides the amount of overlap between diagonal switches, which in turn decides the amount of energy transferred. The diodes on the secondary side of the HF TF (D_{R1} to D_{R4}) provide doubler rectification. L_o and C_o form the output filter, where the inductor is used to limit the current output ripple, while the capacitor is used as a filter to regulate and smooth the DC output voltage[102].

Figure 24 shows the operational waveforms of PWM switching from the switches M1 to M4, and the TF's primary and secondary voltage, respectively. The waveforms are illustrated as ideal due to an ideal TF, which means no resistances, magnetizing inductance, or leakage inductance on the TF, so ZVS is not considered for this principle of operation.
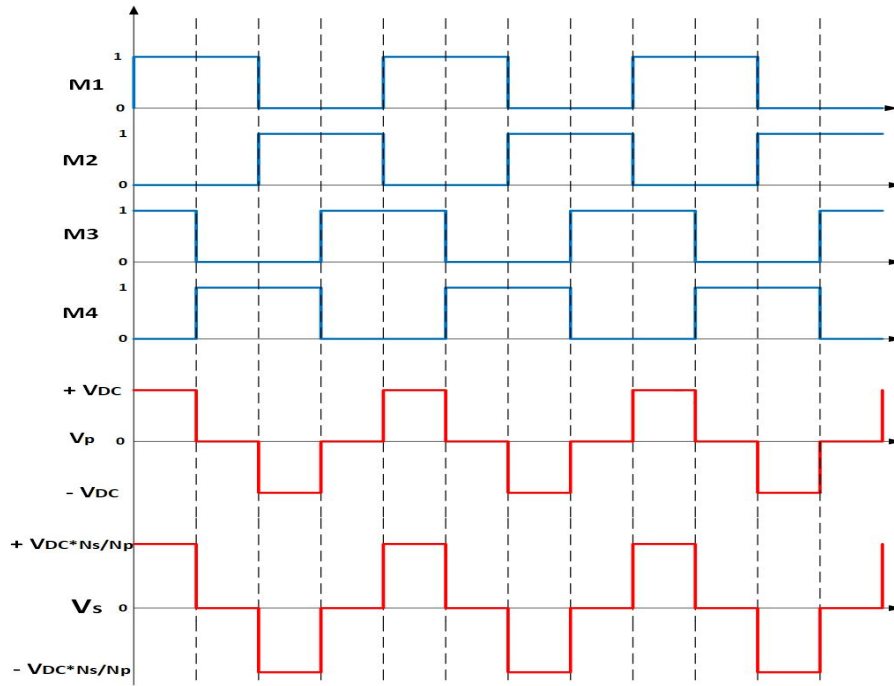
Figure 24: Operational waveforms of the phase-shifted full-bridge DC-DC converter

Seven intervals will explain the first half cycle of the converter's operation. The second half cycle repeats in the same procedure as the first half cycle. The converter has four operating states, determined by the ON/OFF condition of the four switches on the primary side. The state where two diagonally opposite switches are conducting is called the active state, and the state where two switches on the same side of the power bus are conducting is called the passive state. The power transferring occurs only during the active state from the primary side to the secondary side of the TF. The two sets of switches (M1, M3, and M2, M4) operate during different conditions. The converter goes from the active to the passive state whenever M1 and M3 turn OFF. The converter changes from the active state to the passive state after M2 and M4 toggle[95]. The TF is ideal, meaning no resistances, magnetizing inductances, or leakage inductance on the TF.

Interval 1

In this interval, the switches M1 and M4 are ON, and M2 and M3 are OFF in an active power state. The power is transferred from the primary to the secondary side of the TF, as depicted in figure 25. The rectifiers D_{R2} and D_{R3} conduct on the secondary side of the TF. This mode is a power transfer mode, and the primary current flows through M1 and then through M4.
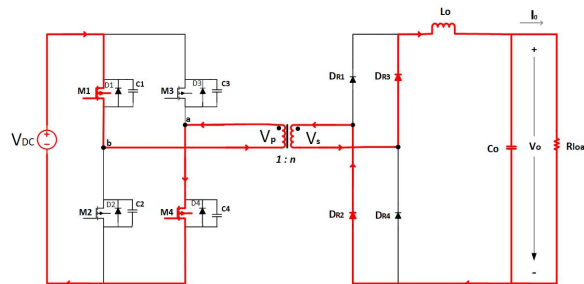
Figure 25: PSFB in interval 1

Interval 2

This mode is a power transition mode from an active state to a passive state, and the active state determines when the switch M1 turns OFF, as determined by the PWM duty cycle. The switch M1 is turned OFF, and since the current flowing on the primary side cannot be interrupted instantaneously, it finds an alternative path. It flows through the parasitic switching capacitances C1 and C2. The primary current charges C1 to V_{DC} and discharges C2 to 0 V, see figure 26.
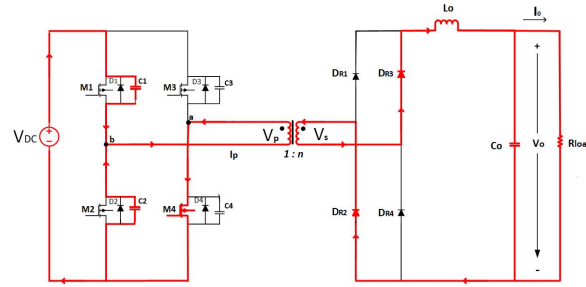
Figure 26: PSFB in interval 2

Interval 3

In this interval, the passive state starts, and all the secondary diodes (D_{R1} to D_{R4}) are free-wheeling. Since the current on the primary side already discharged C2 and charged C1, it forward biases the body diode D2, which can be seen in figure 27.
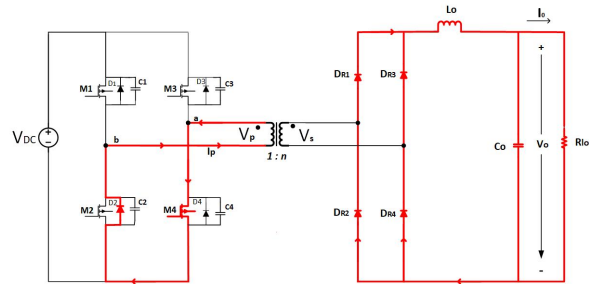
Figure 27: PSFB in interval 3

Interval 4

During this interval, the switches M2 and M4 toggle. The primary current will flow through the parasitic capacitors C3 and C4, which can be shown in figure 28. After the switch M4 is turned OFF, the current flowing on the primary side of the TF charges node a to V_{DC} by charging C4 and discharges C3. In addition, in this interval, the diodes on the secondary side (D_{R1} to D_{R4}) are free-wheeling, and the passive state continues.
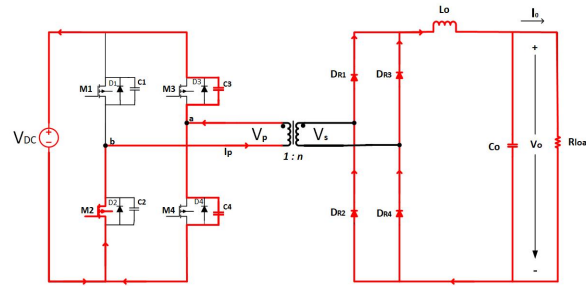
Figure 28: PSFB in interval 4

Interval 5

During this interval, when the parasitic capacitor C3 is fully discharged, the body diode D3 conducts, which can be shown in figure 29. Besides, in this interval, all of the rectifier diodes on the secondary side are still free-wheeling, and the passive state continues.
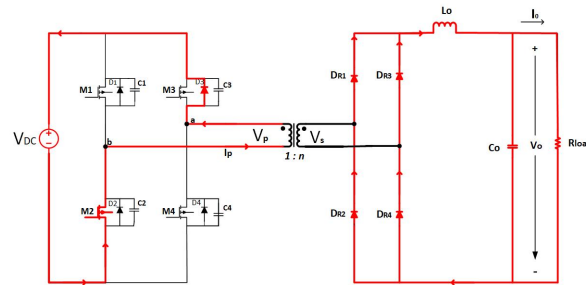
Figure 29: PSFB in interval 5

Interval 6

Under this interval, M3 turns ON, as seen in figure 30, and the polarity of the primary current changes. Besides, all the rectifier diodes are still free-wheeling, and the passive state continues.
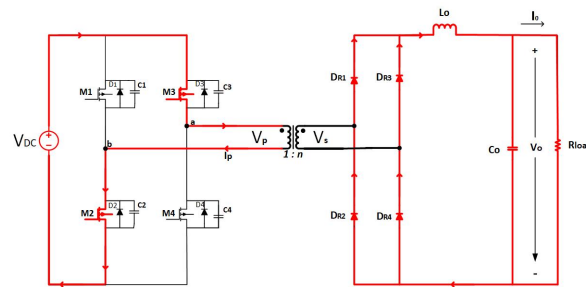
Figure 30: PSFB in interval 6

Interval 7

This interval is a transition mode from passive to an active state after the current through the TF equals the current through the filter inductor (L_o), which is shown in figure 31. The secondary rectifiers (D_{R1} and D_{R4}) start to conduct, and the transfer mode begins again.
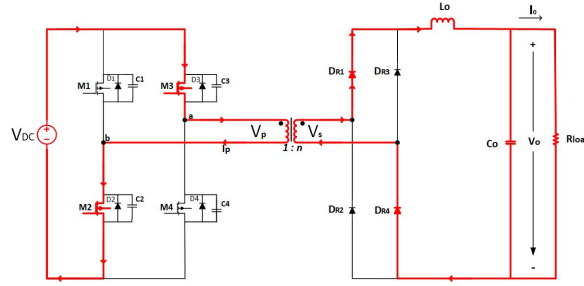
Figure 31: PSFB in interval 7

2.12.3 Design of a Phase-Shifted Full-Bridge DC-DC Converter

HF TFs are designed to support integration with electronic switches in the form of HF signals. Besides, they are designed to achieve the desired output voltage, which is maintained between the lowest input voltage when the maximum load is connected. The duty cycle (D) is a significant factor that contributes to controlling the operation of the system to transfer the energy of the HF TF from the primary to the secondary side[103]. The HF TF's turns ratio n must be decided based on the minimum input voltage and can be defined as[79]:

$$n = \frac{N_s}{N_p} = \frac{1}{2 \cdot D} \cdot \frac{V_{out}}{V_{in,min}} \tag{6}$$

where D is the duty cycle at 50 %, N_p and N_s is the number of turns in the TF's primary and secondary winding, respectively, V_{out} is the output voltage, and $V_{in,min}$ is the minimum input voltage.

The output filter inductor and capacitor values should be calculated based on maximum ripple current and ripple voltage. If considering CCM (inductor current never turns to zero), the calculation of the minimum inductor value ($L_{o,min}$) can be defined as[79]:

$$L_{o,min} = \frac{n \cdot D \cdot V_{in}}{2 \cdot \Delta IL_{max} \cdot f_s} \qquad [\text{H}] \tag{7}$$

By research, a percentage of ripple current of 10 to 30%[104],[105],[97], [106] have been found for PSFB DC-DC converters.

Next, the minimum value of the output filter capacitor ($C_{o,min}$) can be based on the inductor current ripple value and the output capacitor ripple voltage, stated as[79]:

$$C_{o,min} = \frac{\Delta IL_{max}}{8 \cdot \Delta V_{out,max} \cdot f_s} \qquad [\text{F}] \tag{8}$$

In literature for PSFB DC-DC converters regarding ripple voltages, acceptable ripple voltages are less than 2 V for a 3.3 kW onboard battery charger for a plug-in hybrid vehicle, with an output voltage range of 200-470Vdc[107]. In [97], an output voltage ripple of 1 V was designed for a 50 kW PSFB converter for fast charging applications. A HV pulsed power application of 20 kW obtained a controllable load range from 500 V to 20 kV with 0.05% output ripple[108]. In [103] aimed to control the output voltage at constantly 400 Vdc with a ripple output of 0.25 %. Besides, according to NEK410A, the ripple voltage has a tolerance of 10 % in electrical ship installations[63].

According to Ohm's law, a load resistor can be calculated based on the output voltage and current, and can be stated as[11]:

$$R_{load} = \frac{U}{I} \qquad [\Omega] \tag{9}$$

where U and I is the output voltage and current, respectively.

2.13   PID Control

A PID controller can be used in a closed-loop (feedback) system and is widely used in various applications, such as controlling temperatures, pressure, flow rates, electrical systems, etc. The fundamental of the PID controller is that the controller calculates an error, which is the difference between a measured output variable and the desired set-point value. The controller will try to minimize the error by continually adjusting the inputs. In order to have an effective system, the controller must be correctly tuned. A PID controller contains three separate parameters[109]:

The proportional parameter (K_p): is also called gain, and the parameter determines the reaction of the current error. The K_p creates a change to the system's output proportional to the system's current error value. A large K_p-value will result in a significant change in the system's output for a given error and thus can be used to amplify the speed at which the controller reacts to a specific state condition. Nevertheless, if the gain is too large, the system can be unstable, and if the gain is too small, the controller will consequently have a small response to an error value. If the condition is ideal with no disturbances, a purely proportional control system will not settle at the set-point value but will maintain a steady error[109].

Integral (K_i): is the reset loop, and the value contributed from the integral loop is proportional to the duration of error and magnitude. Integrating the error over time results in an offset value that should have been previously corrected. When K_i is added to the proportional term, the integral loop accelerates the response of the process towards the set-point value. It eliminates the residual steady-state error of a P-controller. Since the amount of overshoot is directly related to the value of K_i, a PI-controller will not have the same steady-state error as a P-controller[109].

Derivative (K_d): is the rate loop, where the derivative loop calculates the rate at which the error is changing by calculating the slope of error[109].

2.14   Insulation Resistance of a Battery Pack

The insulation resistance indicates the magnitude of leakage current that flows through a circuit. Since there is no ideal insulation material, there will always be a flowing current within the insulation. Ideal insulation is with infinite resistance, but such materials do not exist. However, in reality, there will be some current that flows through the insulation to the ground or along the insulation[110]. According to ISO 16750-2, the insulation resistance of a battery pack in a vehicle should not be lower than 10 $M\Omega$, so the insulation resistance should always be above this value throughout the battery's operational lifetime[111]. Figure 32 illustrates how a battery's mechanical chassis, which contains insulation resistance, is connected to PE.
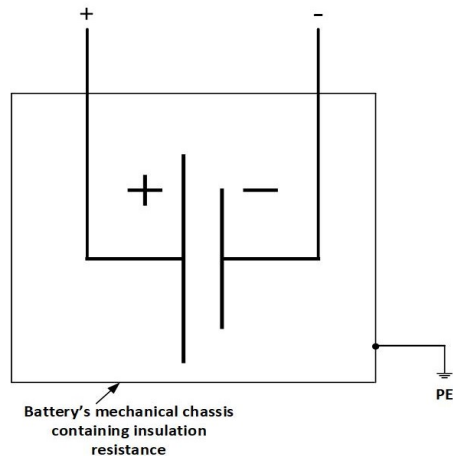
Figure 32: Battery's mechanical chassis connected to protective earth

2.15 Safety Standards

The risk of electrical shock can occur in faulted electrical systems when ECP becomes "live" or if the insulation of the powered conductors is decreasing. If a fault occurs, it is significant to increase the personnel safety by earthing the electrical system[57]. In AC and DC systems, the maximum legal touch voltage is 50 V_{AC} and 120 V_{DC}, respectively. So, equipment that is supplied with nominal voltage exceeding 500 V must have protection against direct touch of live parts in accordance with NEK IEC 60529[63]. Normally, 30 mA through a body with a resistance of 1667 Ω gives less than 50 V maximum touch potential for humans in AC net and a maximum 60 V in DC net[112]. A vital notification is that a leakage current can be much lower than the maximum threshold value for a legal touch current of 30 mA, so it takes incredibly little for corrosion phenomena on the ship's hull.

Another important notification is that the human body is sensitive to (and endangered by) the current and not the voltage. Besides, the human body resistance is not constant but depends on the voltage of the energized object to which the person is exposed to. A nonlinear relationship exists between the voltage and body impedance: the greater the potential difference applied to the body, the lower the body resistance and, therefore, the greater hazard. As a consequence, two different touch potentials will provoke two different body resistances but cause the same current[11].

3 Method

The charging and grounding configurations have been created in the Matlab/Simulink environment and will be explained further in two sections; first, the designed charging structure will be presented, and then the chosen grounding strategy.

3.1 Charging System during Cold Ironing Operation

The charging system from shore and ship-side, which supply the ship's battery (load resistor), can be seen in figure 33. In order to feed the shore-side TF, an AC load supply was implemented into the charging system. Next, a three-phase diode-bridge rectifier converted the AC power into DC power and provided a DC bus. In order to provide galvanic isolation between the ships, an isolated DC-DC converter was designed and implemented on the ship-side. The design of the different components in the proposed charging system for cold ironing operation will be explained in detail further.
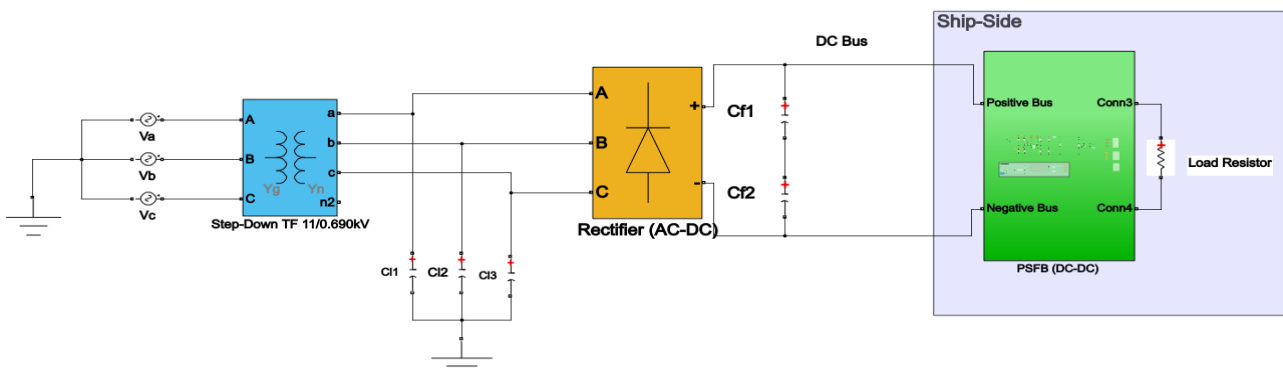
Figure 33: Proposed power supply during cold ironing

3.1.1 AC Power Supply

A star-connected TF was fed with an 11 kVrms three-phase AC supply and was set to step down 11 kVrms to 690 Vrms. The TF's magnetic core parameters were calculated based on open-circuit parameters. The open-circuit parameters of the TF were given, and the parameters can be seen in table 3. In addition, the TF also operates with a rated frequency of 50 Hz, so it was assumed that a frequency converter is not necessary.

Table 3: Open-Circuit Parameters of the Transformer

Open-Circuit Test	
I_{oc} [A]	0.379
V_{oc} [V]	10000
P_{oc} [W]	2800

Based on the given values, R_c and X_m was calculated with equations 1, 2, and 3. The values of R_c and X_m was therefore calculated to 35.7 $k\Omega$ and 39.1 $k\Omega$, respectively. In order to receive enough AC power to the rectifier, the winding parameters on the primary and secondary side of the TF were adjusted through iterations during simulations of the complete charging system.

Next, three equal-valued cable capacitors were added to the shore-side power supply and connected to ground. A smooth and large enough voltage and current out of the TF was obtained by adjusting the values of the cable capacitors through iterations. As a result, the most optimal values for the cable capacitors ($C_{l1} = C_{l2} = C_{l3}$) were 7 mF.

3.1.2 Three-Phase Diode-Bridge Rectifier

The AC power was converted to DC through an uncontrolled three-phase diode bridge rectifier. In Simulink, the block termed Universal Bridge was utilized, and the rectifier uses a six-pulse diode bridge to rectify AC to DC power. Due to grounding purposes, a neutral point of the rectifier's DC output was obtained by two equal-valued filter capacitors (C_{f1} and C_{f2}). The capacitors regulated the DC output voltage and reduced the ripple voltage to an acceptable magnitude. Through iterations, the value of the filter capacitors was 50 mF each. The voltage across the capacitors was measured during simulations to ensure that voltage balance was obtained across the capacitors. A vital notification is that the DC bus voltage will vary when varying the load resistor of the PSFB DC-DC converter since the rectifier is an uncontrolled power device.

3.1.3 Design of a Phase-Shifted Full-Bridge DC-DC Converter

In this paper, a 400 kW PSFB DC-DC converter was designed and is presented in figure 34. Blue Day Technology uses a unipolar DC system in their charging system, appropriate for this type of DC-DC converter. Therefore, this converter uses less components than a bidirectional isolated DC-DC converter with switches on both sides of the HF TF. Instead, this converter uses diodes on the secondary side, and a control system is also only necessary on the primary side. The proposed converter uses MOSFET switches on the primary side. Since this converter is in a high-power rating, SiC MOSFET switches can be used in reality to operate at high voltages and frequencies. In this paper, conventional MOSFET switches from the Simulink library were used. Furthermore, the gating signal of the MOSFET switches is controlled with PWM control pulse generation and will be explained further.
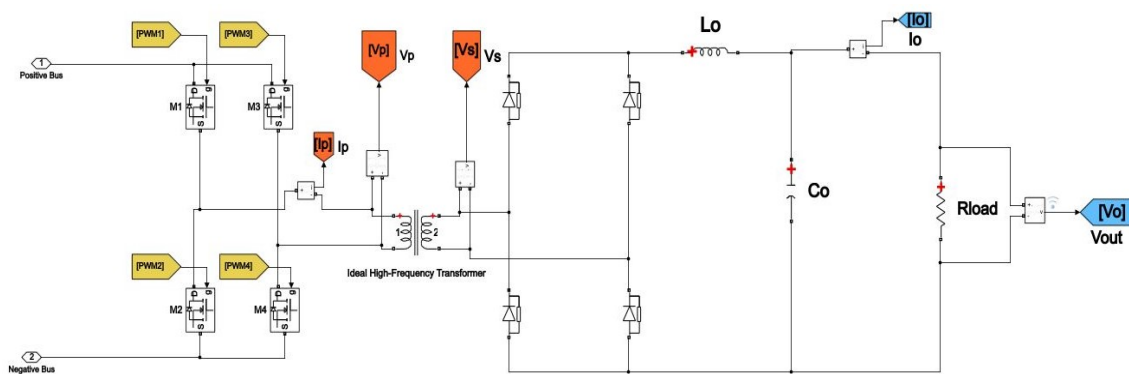
Figure 34: Model of the PSFB DC-DC converter

In this approach, a phase-shift method was applied by feeding back the output signal (V_o) of the converter, as depicted in figure 35. The feedback voltage signal was compared to a constant reference voltage (V_{ref}) to achieve an error signal. The reference voltage was set to 1000 V_{dc}. Next, this error signal passes through the PID controller, and a phase value will be obtained. The PID controller block was found in Simulink. From the output saturation section in the PID control block, the phase value was limited to a range of [1,180°]. The regulated phase is sent to

the PWM function block, which is a Matlab function block that will calculate the phase-shift time (t_{phase}) for the PWM control pulse generation algorithm.
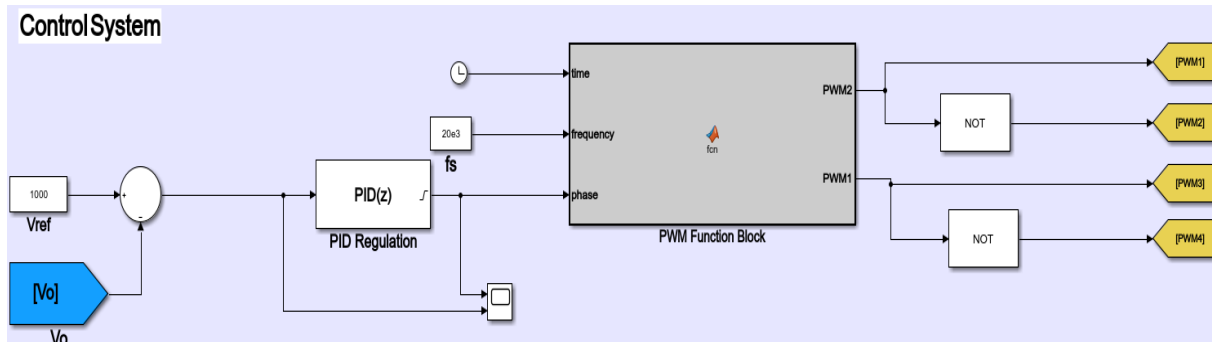
Figure 35: Control system of the PSFB converter built in Matlab/Simulink

The converter is controlled through an algorithm that is described and depicted in figure 36. With this presented approach, two control pulses are obtained for PWM1 and PWM2. Through the NOT gate from the signals from PWM1 and PWM2, the pulse signals for PWM3 and PWM4 will also be controlled. If switch M1 is ON, M2 is OFF, and opposite. Besides, if M3 is ON, M4 is OFF, and the opposite. The response for a voltage change of the converter's control system was verified through a change in the reference voltage from 1000 V to 800 V during a simulation.

Before the PSFB DC-DC converter was implemented with the shore-side TF and rectifier, an ideal DC voltage source was utilized, with a constant input voltage of 800 V_{dc}. Furthermore, the HF TF was constructed as ideal, so the winding parameters on the primary and secondary side were set to 0, and magnetization resistance and inductance were set to infinity. The only designed parameters were the nominal voltage at the primary set to 800 V and the secondary side to 1000 V of the HF TF. The converter is designed to meet the design specifications listed in table 4. Based on these design parameters, the HF TF's turns ratio and minimum values of the filter inductor and capacitor were calculated.
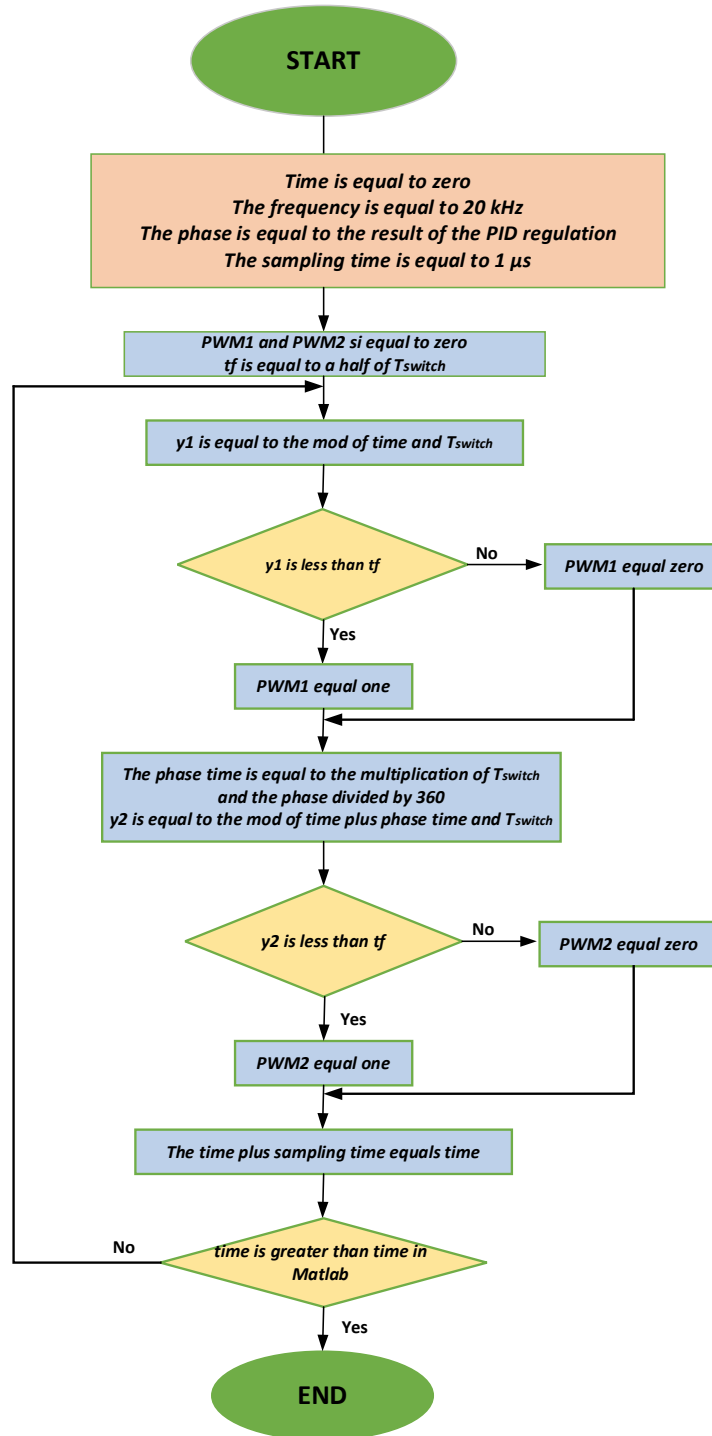
Figure 36: Flowchart of the algorithm for the control of the PSFB converter

Table 4: Design Specifications for Calculation of Filter Parameters

Design Parameters	Value [Units]
Min. Input DC Voltage	800 [V]
Output DC Voltage	1000 [V]
Max. Output DC Current	400 [A]
Max. Output Power	400 [kW]
Output Voltage Ripple (0.25% of Vout)	10 [V]
Output Ripple Current (20% of Iout)	80 [A]
D	0.5
Switching frequency	20 [kHz]

After researching in the literature regarding ripple voltage and current, the percentage of the output voltage ripple and the current was set to 0.25 % and 20 %, respectively. The switching frequency was set to 20 kHz, achieving higher efficiency due to lower switching losses, but the size of the HF TF will be larger. The values of the MOSFET switches were in default values.

The HF TF's turns ratio was calculated to 1.25, based on equation 6. The minimum output filter inductor and capacitor values were calculated with the equations 7 and 8, respectively. Their respective minimum values can be seen in table 5. However, it is not sure that their respective values exist on the market. So, they were compared to realistic values from the websites [113] and [114]. Through simulations in Matlab/Simulink, their most optimal and existing values on the market are seen in table 5. The load resistor, which represents the ship's charging battery, is based on equation 9. At nominal and half load (400 kW and 200 kW), the load resistor will be 2.5 Ω and 5 Ω, respectively. The charging system will be presented during full and half load based on the load resistor.

Table 5: Minimum and Actual Filter Values

Calculated Filter Parameters	Value [Units]	Actual Filter Parameters	Value [Units]
Lo,min	156.3 μH	**Lo**	220 μH
Co,min	200 μF	**Co**	220 μF

Furthermore, during PID tuning, the K_p parameters were first set to a very high value until the output voltage started to oscillate. After that, the K_p value was divided by 2. Next, the K_i parameter was set sufficiently large and adjusted several times so that the overshoot was not too large. Finally, the K_d parameter was set through iterations to obtain a smooth output voltage. The designed PID parameters for the converter can be seen in table 6.

Table 6: Designed PID parameters

K_p	K_i	K_d
$25 \cdot 10^7$	$100 \cdot 10^3$	750

A resistance of 20 Ω was added in series with the PEN conductor's resistor during simulations of the complete charging system from the uncontrolled diode bridge rectifier. Otherwise, there was too large power loss due to the TN-C grounding system. Consequently, it would lead to a lower output voltage and current of the PSFB DC-DC converter during simulations. Furthermore, the presented simulations of the charging system were completed together with the chosen grounding strategy because the grounding system has a significant impact on the charging system's power performance.

3.2 Grounding Strategy during Cold Ironing Operation

The design of the grounding structure can have an impact on the power quality, performance stability, and overall safety of the system, especially under an electrical fault. The grounding configuration will determine the current path during a fault and impact the level of fault current and touch voltage a person is exposed to during a fault situation. However, it is essential to accept that there is no ideal grounding topology. The selection of the grounding method should be based on the factors that impact the chosen grounding structure and, eventually, standards that must be followed. In this paper, the limitation of leakage current on the ship during a fault is significant to obtain personnel safety and limiting the fault current's magnitude on the ship to reduce the equipment damage.

3.2.1 Shore-Side Grounding System

On the shore-side grounding system, a double-grounded TN-C grounding configuration together with a NGR was designed, as depicted in figure 37. The choice of TN-C grounding is because only a PEN conductor is needed since the DC structure from the rectifier and the converter does not contain any appliance body that needs to be grounded. Besides, if a TN-C-S grounding system is needed, this can be obtained if any appliances must be connected to the DC bus. In general, a TN-grounding system also has a sufficient amount of fault current that can be detected, such that if a fault occurs on the shore-side, it will be easier to detect and trip the fault.

Furthermore, a HR NGR was added to the TF's neutral point on the secondary side such that the fault current should be limited to less than 25 A. The value of the NGR is based on equation 4, so the rating of the ground-fault current was adjusted several times to see its effect on the grounding structure during a single ground fault. The minimum and maximum ground-fault current were rated from 5 A to 25 A, respectively. With $I_f = 25A$, the ohmic value of NGR is 15.9 Ω. After that, the cable capacitors were set solidly (directly) to the ground. Double phase-to-ground fault and phase-to-phase fault were also introduced in the AC system to verify the grounding system's performance during a fault.

Next, the rectifier's middle point was directly connected to earth through a PEN conductor. In order to size the ground PEN conductor from the rectifier's derived midpoint to the TF's common ground point, the current rating had to be defined. The nominal power and voltage are 300 kW and 850 V, respectively. With equation 5, the nominal current becomes 353 A. With a rated current of 353 A, the minimum cross-sectional area of the grounding

conductor will be 152 mm^2, according to [115]. Information about values for conductor resistances (in Ω/km) was given in a mail from M.Kozac [116], and the datasheet can be seen in Appendix. Since the ground conductor is made of copper[117], the resistance per kilometer will be 0.0991 Ω/km. The distance was set to 20 m from the TF to the rectifier. The resistance of the PEN conductor will be approximately 2 $m\Omega$.
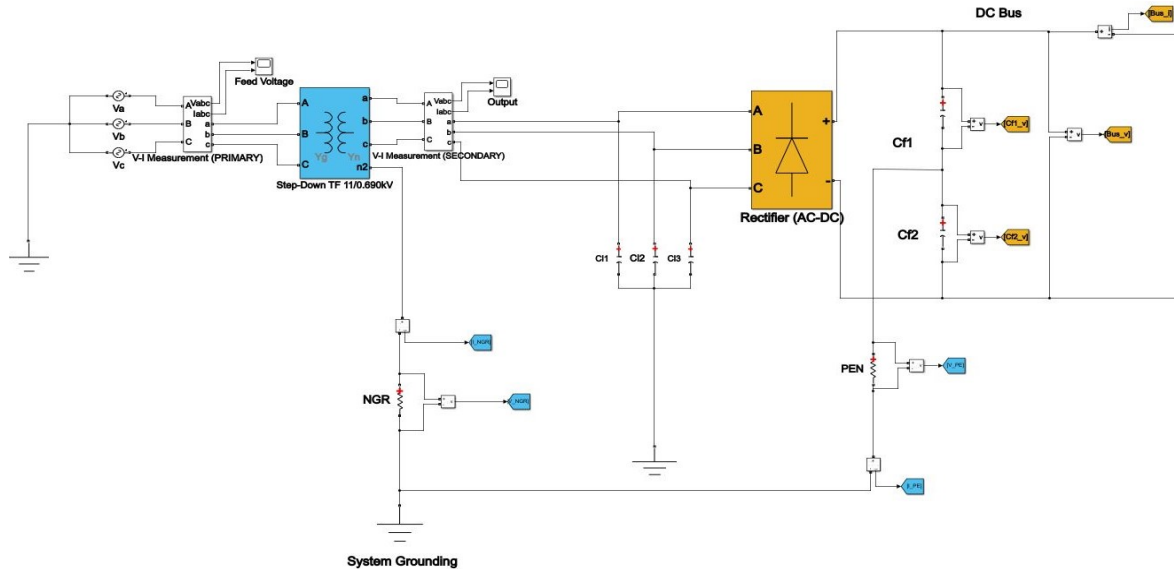

Figure 37: Shore-side grounding system

3.2.2 Ship-Side Grounding System

In order to maintain the galvanic isolation between the PSFB DC-DC converter's input and output, an IT grounding system was designed on the secondary side of the converter, as depicted in figure 38. Therefore, the PE conductor that usually is connected between the shore and ship-side will not be necessary. This will also prevent the ship-side grounding system from being affected by a shore-side ground fault and opposite.

According to Blue Day Technology, the DC-DC converter can be placed on the ship during charging. Therefore, the converter was assumed to be placed on the ship during cold ironing operation. Furthermore, a derived middle point on the secondary side of the converter was created by utilization of two equal-valued HR resistors ($R_{G1} = R_{G2} = 167k\Omega$). Due to voltage dividing, they will form 500 V across each of the resistors. Their derived midpoint, which will provide zero voltage in the middle, was solidly connected to ground. The HRMG resistors operate as HR grounding resistors, providing low leakage current during a LG fault. From Ohm's law, the leakage current during a fault will be a maximum of 6 mA, which is seen as a safe touch current for personnel. Besides, these grounding resistors will prevent energy loss during normal operation and a LG fault, as described in the theory-section.

In order to utilize a high-resistive IT grounding configuration on a ship without a PE conductor to the shore-side, it is essential to emphasize that monitoring devices must be used in reality to alarm the first ground fault. As a result, it will prevent that a large amount of leakage current flows through the ship hull and to the other ships or the quay. However, in this paper, a monitoring device has not been considered during the grounding system's design in Matlab/Simulink.

Moreover, the battery's body (chassis) is grounded separately to PE because of the IT configuration. Due to safety purposes, the chassis of the battery is constructed with a fixed insulation resistance working as a mechanical chassis

that can become energized during a fault. Since insulation resistance on a battery pack for vehicles must be larger than 10 $M\Omega$, the insulation resistance (R_{ib}) was set to an arbitrary value of 30 $M\Omega$. A switch was implemented on the insulation resistance. When a fault was introduced on the ship-side, the insulation resistance was connected to PE. The insulation resistance was connected to the negative DC conductor.
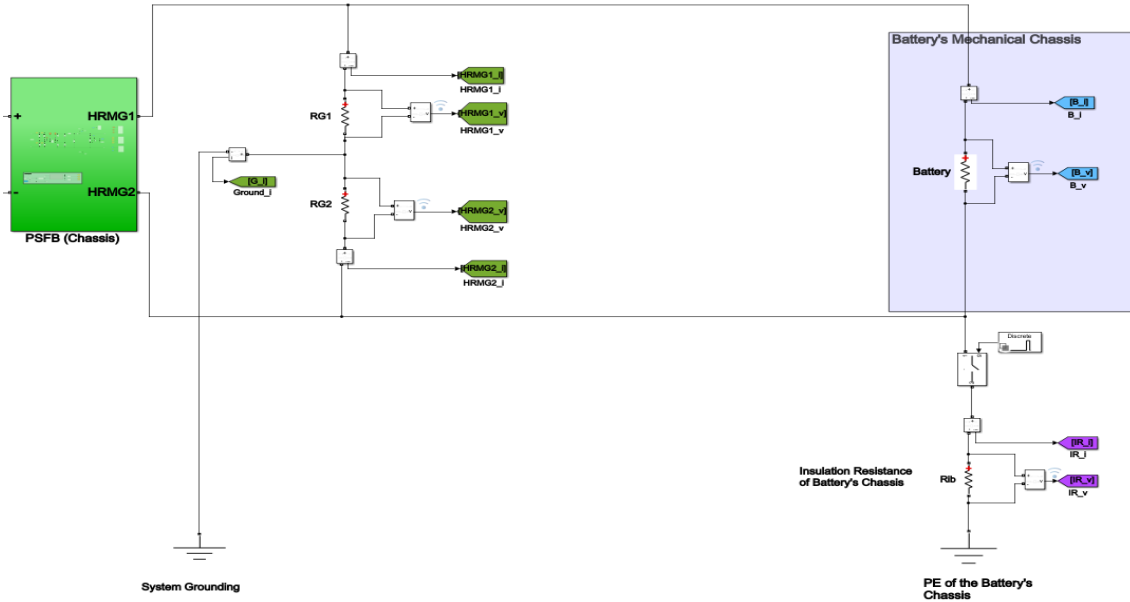

Figure 38: IT grounding system on the ship-side

3.2.3 Introduction to Faults on the Electrical Charging and Grounding System

Regarding how the proposed grounding system corresponds to faults in the electrical charging system, faults were introduced both on the shore-side and ship-side. The location of the simulated faults on the charging system can be seen in figure 39. Only one fault was introduced at a time during simulations. Since one of the targets of this paper was to investigate the different faults that can appear in the power system, different types of faults that exist on the AC and DC side were found through research and are described in the theory section.

When an AC fault was introduced on the AC side, the Three Phase Fault block in Simulink was used with an external switching mode. In the Three Phase Fault block, the fault resistance was set to 0.001 Ω, and the ground resistance was set to 0.1 Ω. According to the description regarding the Three Phase Fault block in Simulink, the ground resistance must be set to a low value when implementing a fault between a phase and ground[118]. The lower the fault resistance, the higher the fault current will become. Next, the external switching device was a Stair Generator block in Simulink, and the block introduced a fault after 0.5 s and lasted in 100 ms.

LL and LG faults were introduced to both grounding systems in the DC-distributed system. The faults were introduced on the DC bus and the DC-line between the PSFB DC-DC converter's output and the load resistor (battery). The LG fault resistance (R_f) was set to a low-impedance fault, with an ohmic value of 0.01 Ω. A fault on the AC or DC system was always introduced after 0.5 s and lasted in 100 ms. In a LG fault, the fault was set on the positive conductor. A simulation of a LG fault was also performed with a body resistance of 1667 Ω touching the battery's mechanical chassis. A LL fault is a low-impedance fault since the conductors are directly connected to the fault[44], so the fault resistor during a LL fault was also set to 0.01 Ω.

The load was set to full load during simulations of a fault. The charging system operates at full load before and after a fault. The simulation type was set to discrete from the powergui block in Matlab/Simulink, and the sample time was 1 μS. The solver selection was a fixed-step, which is required for code generation.
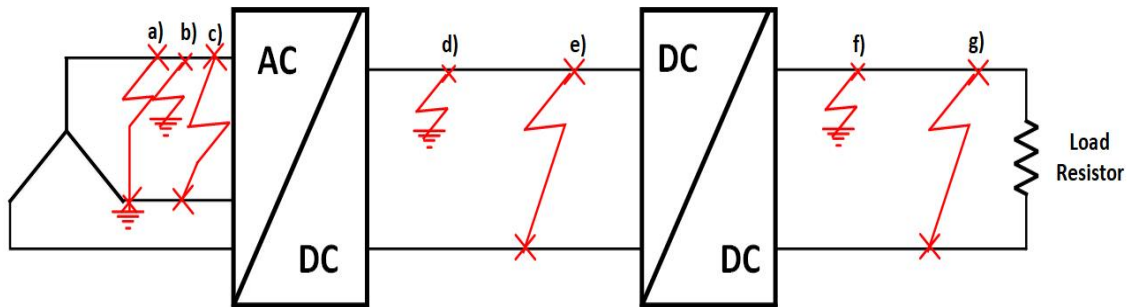

Figure 39: Location of the faults on the charging system, where a) is a double phase-to-ground fault on the secondary side of the shore-side TF, b) is a single phase-to-ground fault, c) is a phase-to-phase fault, d) is a LG fault on the DC bus, e) is a LL fault on the DC bus, f) is a LG fault on the ship-side DC system, and g) is a LL fault.

4 Results and Discussion

4.1 Charging System

The simulations of the charging system are introduced with the whole grounding system because, in general, a grounding system can have an effect on the power performance during normal conditions. The meaning of normal condition means that there is no intentional fault introduced in the system. The operational waveforms of the PSFB DC-DC converter will be presented at nominal load.

Figure 40 showcases the DC bus output voltage from the rectifier and the operational waveforms of the PSFB DC-DC converter under nominal load in steady-state. The average DC output voltage from the rectifier is 953 V. The output ripple from this output became 18 V. In reality, the company's DC bus is at a nominal voltage of 800 Vdc. However, the DC bus voltage will vary since a diode rectifier is an uncontrolled power converter. Next, the PWM waveforms from M1 to M4 can also be seen in the figure, and the waveforms switch between 0 and 1. It can be seen that M1 and M3 are 180 ° out of phase from M2 and M4. The phase shift is most visible from the figure when comparing M2 and M4. There is a bias between M1 and M3 due to the designed sample time at 1 μs. The converter did not obtain the designed phase shift of 50 %, which indicates that the energy transferred is much lower than the designed.

The HF TF's primary voltage (V_p) and current (I_p), and the secondary voltage (V_s) at nominal load is also seen in figure 40. The voltage across the HF TF's primary winding is +837 V_{dc} when the switches M1 and M4 are ON. When the switches M1 and M3 are ON, the HF TF is short-circuited, such that the voltage across the HF TF's primary winding is 0. Next, when M2 and M3 are ON, the output voltage of the HF TF is -837 V_{dc}. The voltage across the HF TF's primary winding is higher than the designed input voltage of 800 V because of the output voltage delivered from the three-phase rectifier. The transferred voltage across the secondary windings of the HF TF is +1047 V_{dc} and -1047 V_{dc}. Therefore, the value across the secondary winding matches that the secondary voltage is 1.25 times larger than the primary voltage.

Moreover, the primary current reaches 504 A to reach the output inductor current ($400A \cdot 1.25$) when the diagonal

switches M1 and M4 are ON. The primary current flows in the negative direction (-504 A) when the diagonal switches M2 and M3 are ON. The waveforms of the primary voltage and current and the secondary voltage are as expected since the TF is ideal, which creates ideal waveforms.
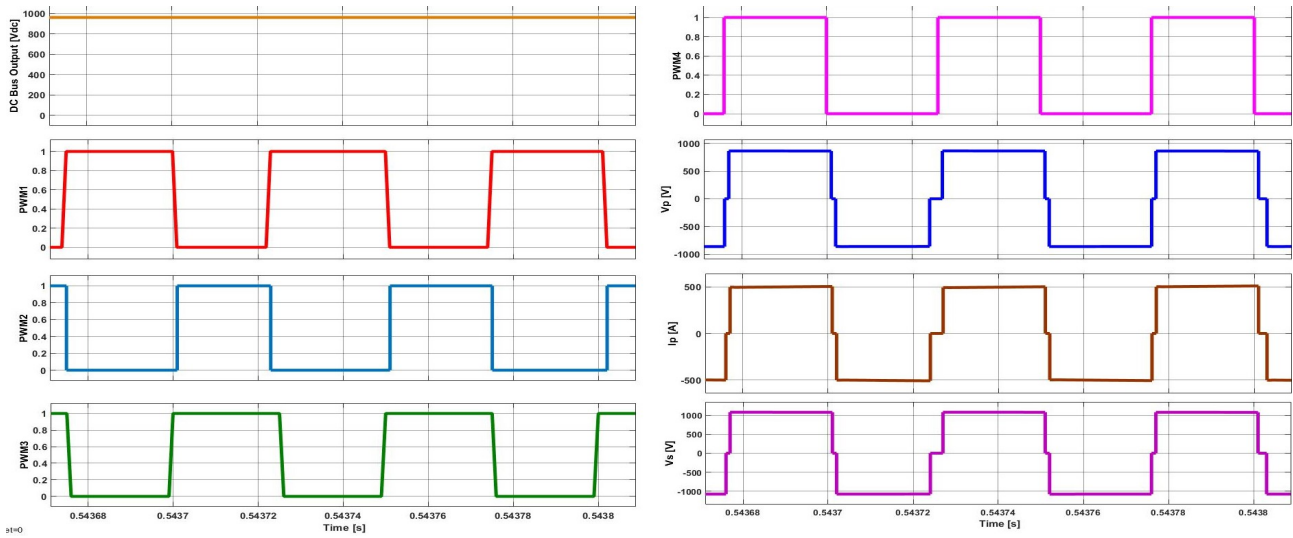
Figure 40: Operational waveforms of the rectifier and PSFB DC-DC converter

Figure 41 shows the voltage across C_{f1} and C_{f2} during normal condition at full load with a simulation time of 10 s. At steady-state, the voltage across the filter capacitors remains simultaneously. The voltage across the capacitors was also simulated at a larger period of 30 s. The voltage across the capacitors neither increased nor decreased; they kept at the same level. However, it has to be pointed out that the voltage across the filter capacitors was with the added resistor of 20 Ω on the PEN conductor such that the power dissipation was not too high.
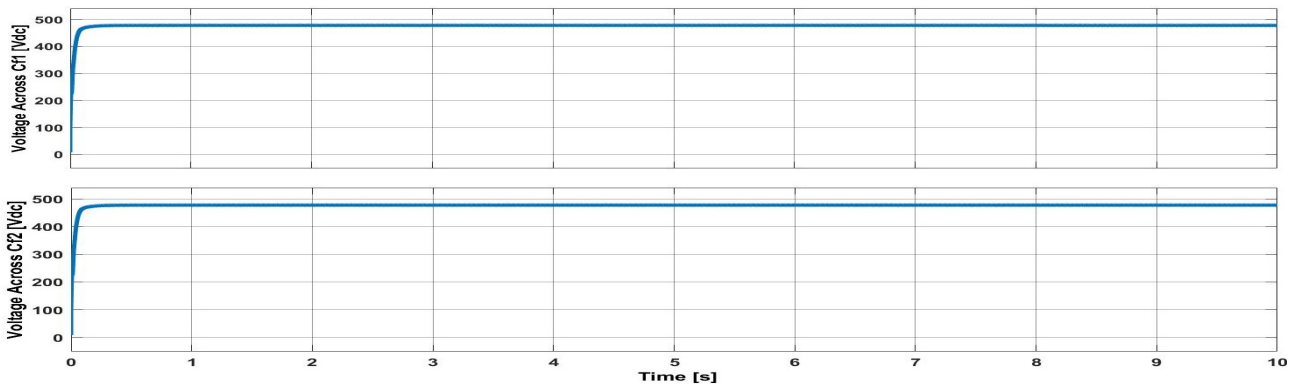
Figure 41: Voltage across C_{f1} and C_{f2} during nominal operation

Figure 42 shows the load resistor's voltage and current during nominal conditions. The isolated DC-DC converter obtains the desired output voltage and current of 1000 V_{dc} and 400 A with acceptable ripple output, which will be presented further in the results. As seen from the figure, the IT grounding on the ship-side with HRMGs does not affect the DC output in steady-state during normal conditions and gives insignificant power dissipation.

Figure 42: Voltage and current of the load resistor during normal condition

Figure 43 shows the DC bus voltage and DC output voltage and the current of the PSFB DC-DC converter during half load in steady-state. The DC bus output voltage ripple under this condition was measured to a ripple of approximately 12 V under steady-state. The ripple is less than during nominal load, but the DC output voltage has increased to approximately 1325 V_{dc}. However, if the magnitude of the DC bus voltage was lower, the DC bus was more unstable, which gave an unstable PSFB DC-DC converter. As seen from the DC output voltage and current of the DC-DC converter, the converter obtains to operate at half load.
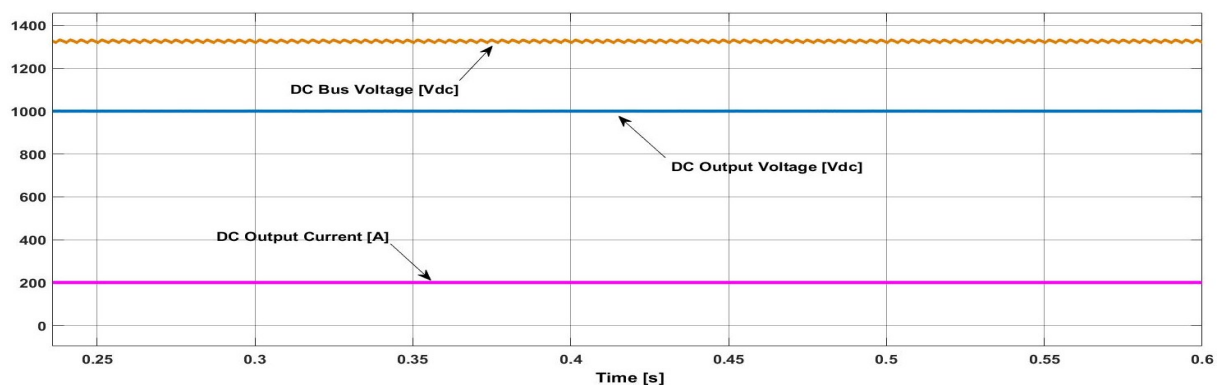
Figure 43: DC bus output voltage and DC output voltage and current of PSFB DC-DC converter during half load

The output voltage ripple and ripple current in the steady-state of the PSFB DC-DC converter under nominal, and half load can be seen in the figures 44 and 45, respectively.

During operation with nominal load, the control system of the converter obtained to give a maximum voltage ripple of 0.15 V. This is less than the designed of 0.25 V. The ripple current at nominal load fluctuates between 400 A and 399.58 A, giving maximum ripple current of 0.42 A.

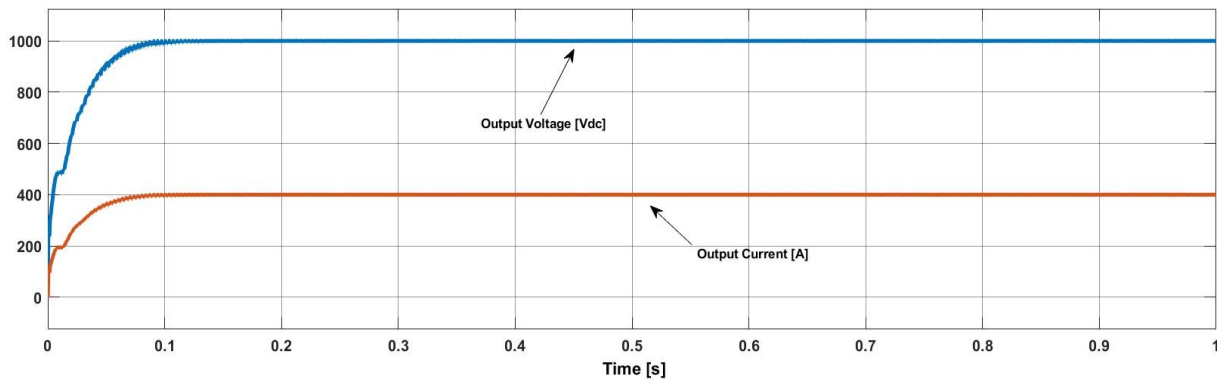During half load, the DC output voltage gives a maximum ripple voltage of 0.5 mV. The output current is reduced to 200 A since the load resistor has been increased to 5 Ω, and the maximum ripple current became 0.12 mA.

Overall, the performance of the PSFB DC-DC converter is affected by the uncontrolled DC bus voltage. Since the rectifier's DC bus voltage delivers higher voltages than designed, the PSFB DC-DC converter has lower output ripple voltage and current than when the converter was simulated with only an ideal DC voltage source. This verifies the reason for the low energy transfer from the primary to the secondary side of the HF TF, which was seen from the amount of phase shift. The DC-DC converter is designed to convert a low input voltage to higher

voltages, but the voltage is decreased to a lower value at half load.
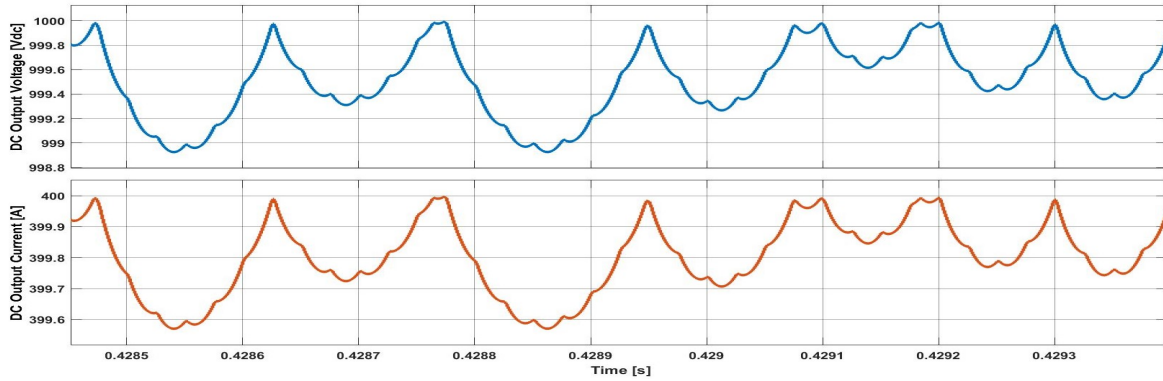
Figure 44: DC output voltage and current under nominal load
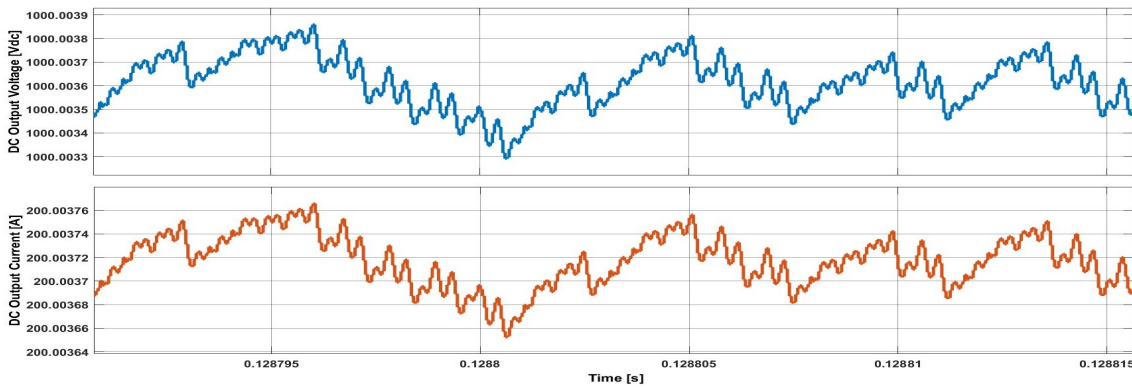
Figure 45: DC output voltage and current under half load

Figure 46 shows the response time of the PSFB DC-DC converter from start-up to steady-state. The converter reaches steady-state after approximately 0.14 s. The response of the converter's control system needs time to reach steady-state because of the large power and grounding system. The TF on the shore-side needs time to reach a stable output. Besides, the K_d parameter of the PID tuning also affects the output from start to steady-state. The start-up is, therefore, slower with the K_d parameter.
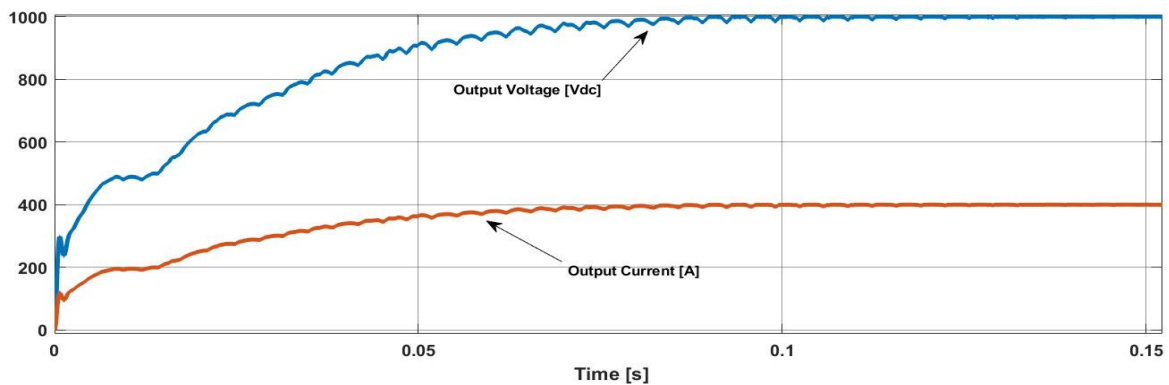
Figure 46: Response of the PSFB DC-DC converter

Figure 47 shows the response of the converter when adjusting the reference voltage from 1000 V_{dc} to 800 V_{dc}. The converter uses 2 ms to reach 800 V_{dc} in steady-state, so it confirms that the control system works and responds when the reference voltage is adjusted.
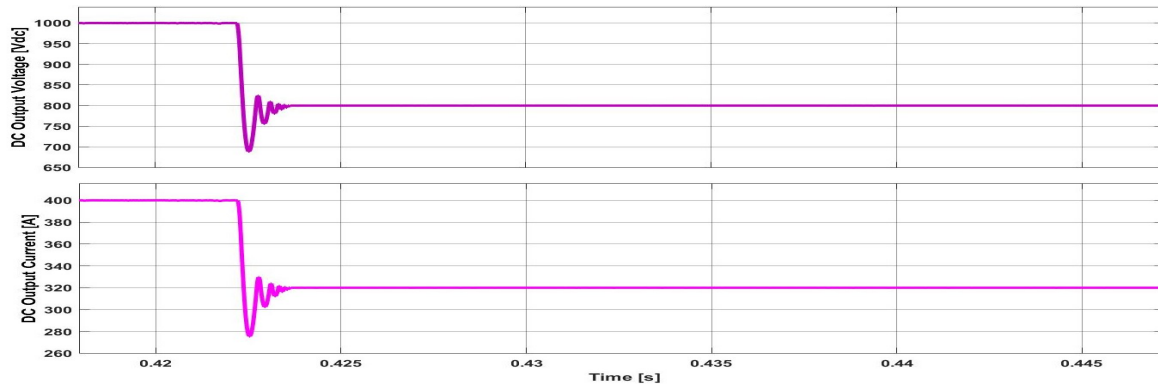
Figure 47: Response of the PSFB DC-DC converter from 1000 V_{dc} to 800 V_{dc}

4.2 Grounding System

Simulations of the shore-side and ship-side grounding system will be presented during normal condition, single and double phase-to-ground fault, phase-to-phase fault, LG fault, and LL fault. The simulation results of the grounding system are divided into two sections; shore-side grounding system and ship-side grounding system.

4.2.1 Shore-Side Grounding System

Normal Operation

Figure 48 shows the voltage and current across the NGR and PEN conductor during normal conditions. A CMV is verified by the voltage across the NGR and PEN conductor because it is not zero potential between the neutral resistors and the common ground point. The voltage and current through the NGR reach 50 V and 4 A, respectively. There is a voltage drop across the NGR because of the cable-to-hull capacitors and the equal-valued filter capacitors that are leaking current to the ground. This creates an arising voltage potential from the ground. Furthermore, from the large current of the PEN conductor that reaches 1000 A and with a voltage across the PEN conductor reaching 2 V, it can be confirmed that the diode bridge rectifier is suffering from a large power dissipation of approximately 1.6 kW.

Suppose a LR grounding resistor of 20 Ω had been added to the PEN conductor. In that case, the power dissipation could have been reduced to 432 W. Therefore, a LR grounding resistor should have been implemented as a grounding device to reduce the amount of power dissipation which will also reduce an eventual fault current on the DC-side. However, the AC and DC shore-side power system are not electrically isolated from each other when a fault occurs (neither with CBs nor an isolated three-phase rectifier). Therefore, a LR grounding resistor could not be added to the PEN conductor during simulations of the shore-side grounding system under normal and fault conditions.

Figure 48: Voltage and current across NGR and PEN conductor during normal operation.

AC Fault

Figure 49 shows the voltage and current across the NGR and PEN conductor, the DC bus voltage, and the fault current flowing out from ground-connected cable capacitors, and the DC output voltage and current of the PSFB DC-DC converter during a phase-to-ground fault. The fault current out from the cable capacitors (I_c) from the figure is flowing out to and to the common ground point. The current from the capacitors is very high in a very short period of 2 μ s, and the fault current has a peak magnitude of 38 kA due to the low fault resistance before it fluctuates from 0 to 1.1 kA. Due to the very high peak on the fault current, the NGR did not reduce the fault current's magnitude to a safe value to prevent damage to the equipment. In reality, a ground fault relay would have been tripped during such a high fault current, but such safety was not considered during the grounding system design. Moreover, the voltage and current of the NGR reach 200 V and 14 A, and the waveforms during the fault have been distorted.

Because the fault current is higher than the maximum of 25 A, the NGR did not achieve to reduce the fault current to the designed value. As a comment, the TF's winding parameters were adjusted through iterations when the rectifier and PSFB converter was implemented into the charging system. Therefore, the output voltage and current of the TF become higher, and the sizing of the NGR has not been correctly designed. Furthermore, the PEN conductor has also been affected by the single phase-to-ground fault, and the PEN conductor voltage and current reach 2.3 A and 1200 V. It can be seen that its respective waveforms have been interrupted due to the AC power. From the figure, the DC bus voltage is disturbed by the phase-to-ground fault, which will affect the DC output of the PSFB converter.
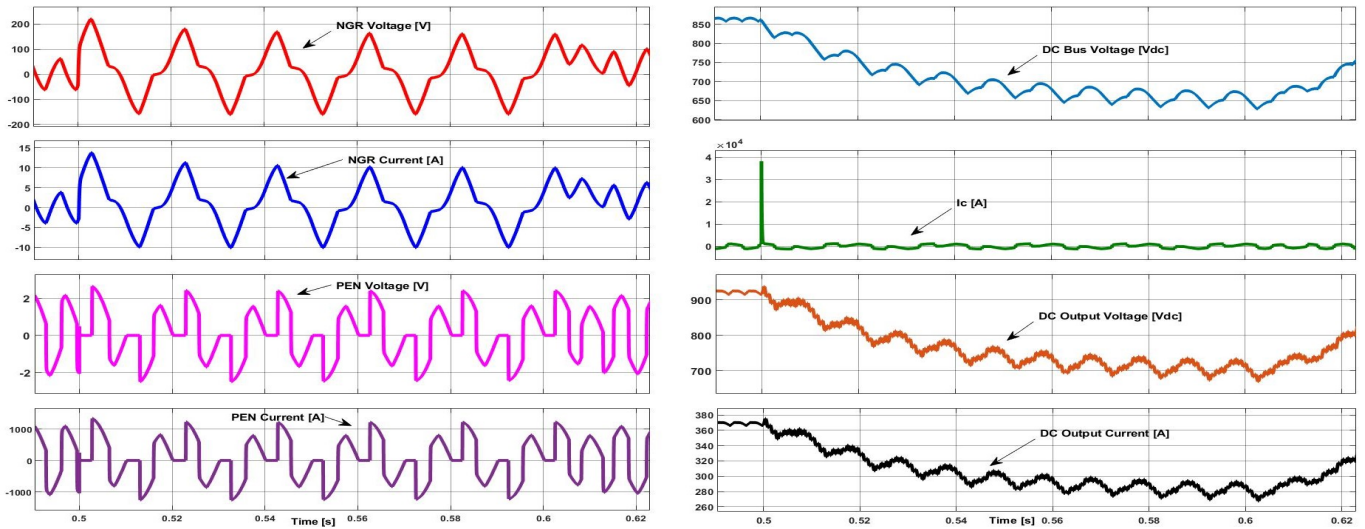
Figure 49: Voltage and Current across NGR and PEN conductor during a single phase-to-ground fault

Figure 50 shows the voltage and current of the NGR and PEN conductor, the DC bus voltage, the fault current through the capacitors, and the DC output of the PSFB converter during a double phase-to-ground fault. The peak value of the fault current reaches 38 kA, which was measured from the AC-line on phase A and phase B. Some of the fault current flows down the cable capacitors (Ic on the figure), reaching a value of 1.4 kA. Next, the voltage and current of the NGR reach a maximum of 150 V and 10 A during the fault, and the PEN conductor reaches 2.5 V and 1.1 kA. Due to lower resistance, there will be more fault current through the PEN conductor than the NGR. The waveforms of the PEN conductor are also distorted. The DC bus voltage decreases during the double phase-to-ground fault because two phases on the AC lines are disturbed by the fault,
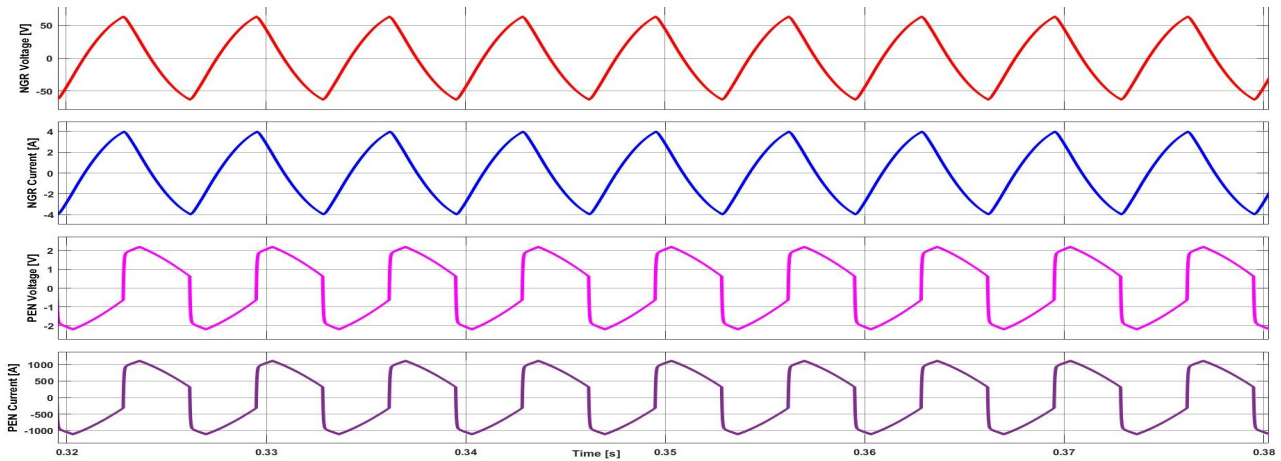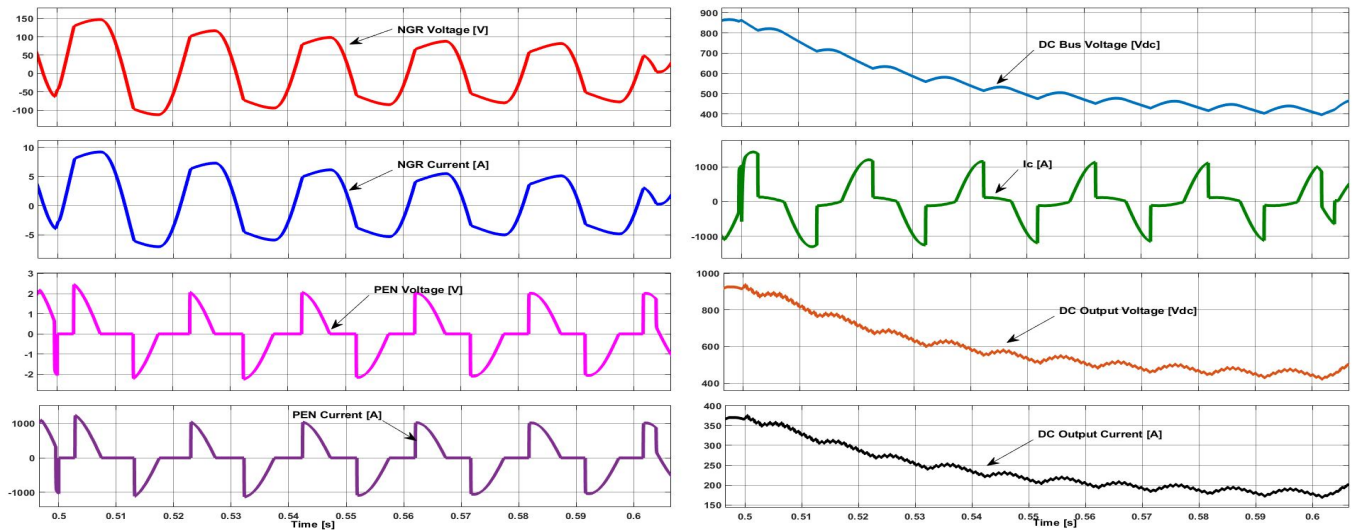

Figure 50: Voltage and Current across NGR and PEN conductor during double phase-to-ground fault.

Figure 51 shows the voltage and current of the NGR and PEN conductor, the DC bus voltage, the current through the capacitors, and the DC output of the DC-DC converter during a phase-to-phase fault. The fault currents of phase A and B have a transient current of 350 kA. Since this is a phase-to-phase fault, the amount of fault current is not flowing to the grounding system, and this scenario is therefore seen as a hazardous situation in reality. The NGR and the PEN conductor's waveforms have been interrupted due to the fault. The operation of the rectifier is

also interrupted due to the AC waveforms. Two of the phases collapse during a phase-to-phase fault, such that the performance of the DC-DC converter decreases.
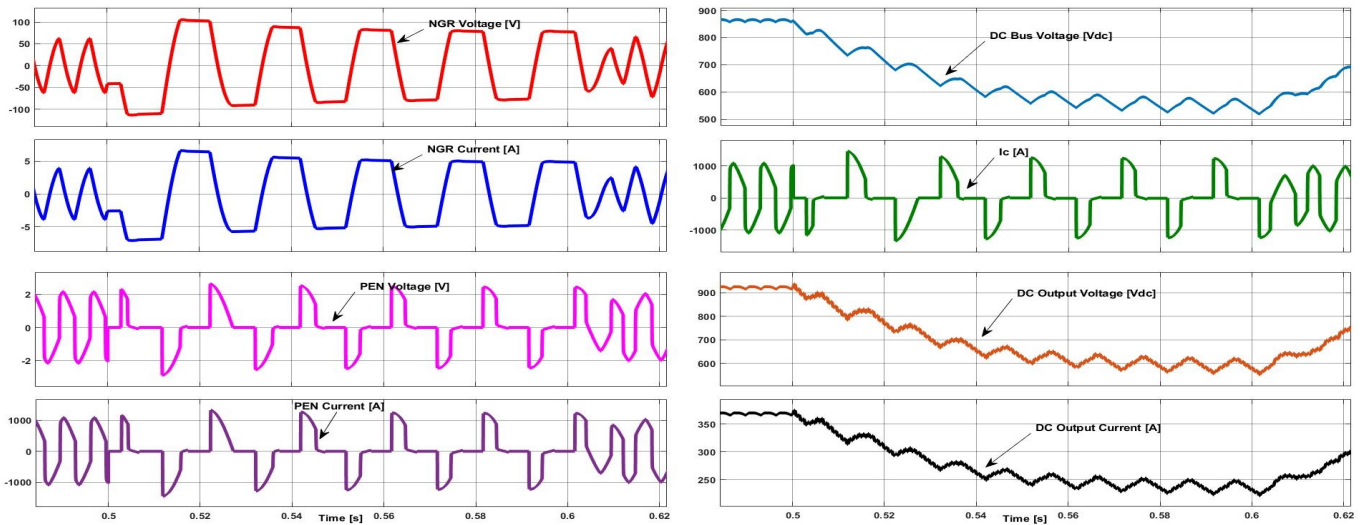
Figure 51: Voltage and Current across NGR and PEN conductor during a phase-to-phase fault

Line-to-Ground Fault

Figure 52 shows simulations of a LG fault, the waveforms presented are the voltage and current of the NGR and the PEN conductor, the fault current, DC bus voltage, the current that flows through the cable capacitors, and the DC output voltage and current of the load resistor. The voltage and current of the NGR increases during the fault. Nevertheless, since the transient current of the fault current reaches 38 kA, the NGR has not achieved to reduce the fault current to a maximum of 25 A. A large amount of current is flowing through the PEN conductor with a peak value of 28 kA, and a significant amount of fault current is also through the grounded capacitors. The LG fault decreases the voltage of the DC bus since the DC bus is grounded through a low impedance of the PEN's resistance of 2 $m\Omega$. This results in a high fault current; consequently, the DC output of the PSFB DC-DC converter is also affected.

It has to be pointed out that an additional LR grounding resistor was not added in series to the PEN conductor because the intention with the LG fault is that the fault current should go back to its respective power source. In this case, the AC/DC rectifier, through the PEN conductor and not through the NGR and the cable capacitors connected to ground. However, the shore-side grounding system is not galvanic isolated from each other nor isolated with CBs nor fuses such that they share the same common ground point. Therefore, it is difficult to lead the fault current occured on the DC bus back to the neutral point of the rectifier through the PEN conductor. Since the fault current takes the lowest path, the PEN had to be lower than the NGR such that much of the current flows through the PEN conductor. However, since the cable capacitors has a lower conductive path, a significant amount of the LG fault current flows upward them as well. From this specific simulation, it can be stated that the AC and DC side should have been isolated from each other during a fault.
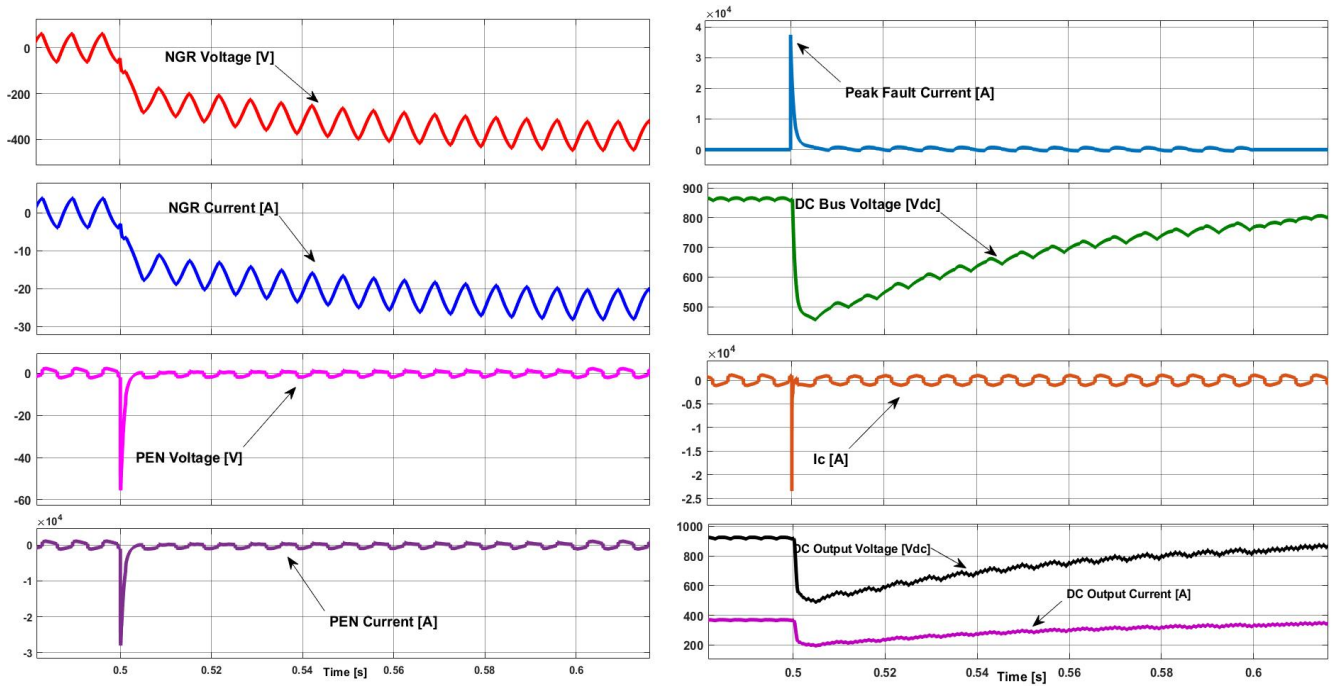
Figure 52: Shore-side line-to-ground fault

Line-to-Line Fault

Figure 53 shows the NGR's voltage and current, the PEN conductor's voltage and current, the fault current, the DC bus voltage, the current flowing through the cable capacitors, and the output of the PSFB DC-DC converter. As seen on the fault current's magnitude, it reaches a peak current of 80 kA, and the fault lasts in a time of 1.4 ms and then fluctuates between 0 and 15 A. The high fault current is due to that the filter capacitors are discharged during the fault, and therefore releasing a large amount of current. The current from the ground-connected capacitors reaches approximately 200 A. There is a very small voltage potential and current from the NGR with a maximum of 2 V and 0.1 A.

The voltage and current of the PEN conductor reach 0.4 V and 200 A, respectively. The waveforms of the PEN conductor have been distorted due to the fault. The DC bus voltage collapsed when the fault occurred, which naturally affects the DC output of the PSFB DC-DC converter. All in all, there is almost nothing of the fault current that flows through the grounding system. As a result, the grounding configuration does not contribute to safety during LL fault, as also stated from the theory-section
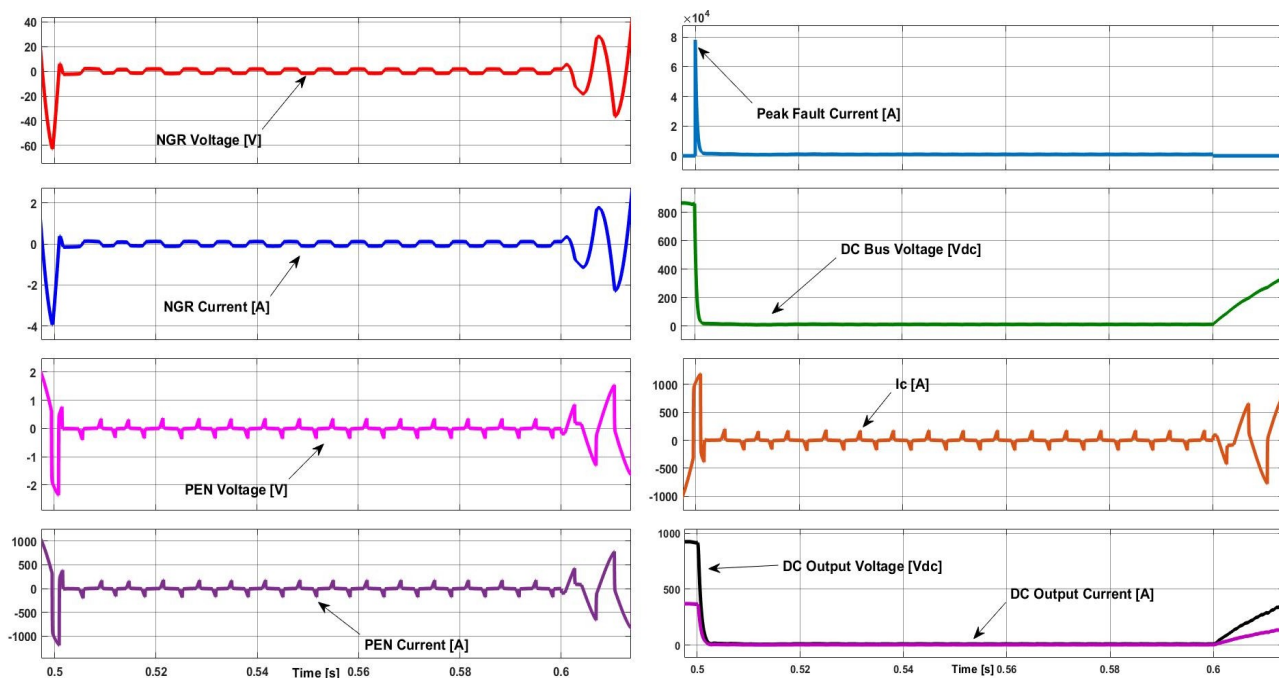
Figure 53: DC bus voltage, ground current through PEN conductor, and fault current during a LL fault

4.2.2 Ship-Side Grounding System

The simulation results of the ship-side grounding system will first be presented during normal conditions with no faults, then a LG fault, and finally, a LL fault is introduced.

Normal Condition

Figure 54 shows measurements of the voltage and current of the grounding system during normal operation. Due to voltage dividing and Ohms law, the voltage is 500 V with respect to ground, and the current reaches 3 mA for each of the HRMG resistors.
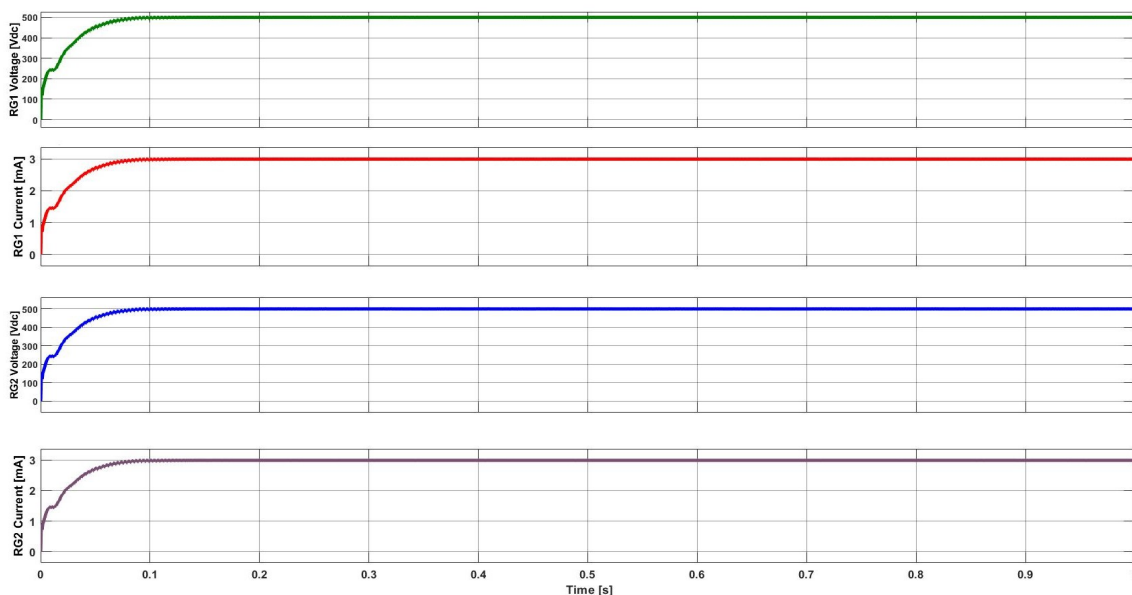
Figure 54: Voltage and current of the grounding system during normal operation

Figure 55 shows the ground current that is solidly connected to earth from the middle point of the HRMG resistors. It can be confirmed that, under normal condition, no current will flow to earth, as long as the HRMG resistors are equally.
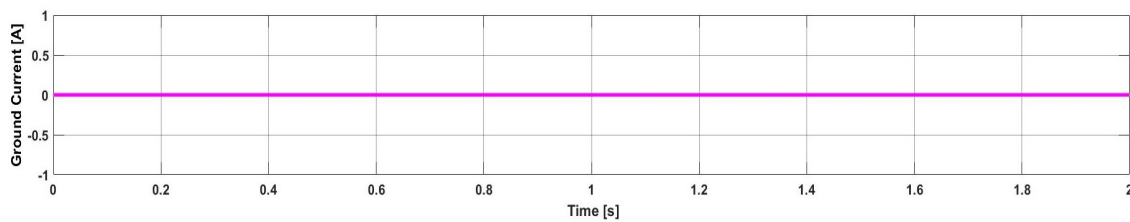
Figure 55: Ground current during normal operation

Line-to-Ground Fault

Figure 56 shows the voltage and current measurements of the HRMG resistors, the ground current, fault current, the current through the insulation resistance, and the output voltage and current of the PSFB DC-DC converter during a LG fault on the positive pole of the supply. Due to the fault on the positive pole, the negative (healthy) pole is forced to handle the entire voltage and current at 1000 V and approximately 6 mA, respectively. As a comment, insulation materials on the conductive electrical wires should be large enough to tolerate full DC voltage[5], so the insulation materials should be designed to handle at least 1000 V_{dc}.

The ground-fault current from the low-impedance has a rating of 6.021 mA. Because of the ripple, the ground fault current will vary with a minimal value. Further, most of the fault current flows to the ground point in the middle of the HRMG resistors, or more precisely 5.988 mA. The remaining goes to the PE of the insulation resistance, or more precisely 0.033 mA. Since the leakage current also flows to the mechanical chassis, it indicates that the chassis has become energized with a voltage potential across the insulation resistor. Even though the fault current flows upward in the system's ground conductor and in the PE conductor of the insulation resistance, it is not certain that the leakage current will flow back into the grounding system again. The ground conductor and the PE conductor are earthed to the ship's hull, such that there will be a circulating current on the ship's hull, creating a voltage potential among the ships.

If the fault resistance were 800 Ω as a worst-case scenario for a human[53], the only difference from a low-resistance fault resistor would be the voltage across the fault resistor. This is because the HRMG resistors will always keep the fault current at a value of 6 mA unless one of the HRMG resistors are disconnected from the grounding system. An important notification is that the HRMG resistors must always have the precisely same values; otherwise, the zero voltage potential between their derived midpoint and ground is broken.

Furthermore, with equation 9 and with a fault current and resistance of 6 mA and 800 Ω, respectively, the voltage potential the person is exposed to will be 4.8 V. If this scenario had been a human touching the positive DC conductor with reference to ground, the person would not have been in danger to electric shock. It has to be pointed out that if a person had been exposed to this scenario, there must have been damage to the wire's insulation material that led to this fault.

The figure also showcases the DC output voltage and current of the PSFB DC-DC converter during a LG fault.

From the figure, it is hard to notice if there is a LG fault in the power system. The ship-side charging system enables fault-ride-through capability of a LG fault, but on a ship, it will lead to a circulating current that will flow out of the ship's hull and into the sea to the other ships and the quay.

If an IT grounding system is going to be utilized on a ship, the LG fault must be cleared as soon as possible to prevent corrosion derived from leakage current. Even during a LG fault, a fault ride-through is not recommended on a ship to prevent voltage potentials between the ships and the pier. IMD is, therefore, a must such that if the insulation resistance of the HRMG resistors decreases, an alarm will be triggered. In addition, a vital notification is that the voltage across each of the resistors should be monitored continuously. If one of the resistors has the full voltage, a LG fault has occurred. The power system should therefore be shut down through the first LG fault to prevent an increase in leakage current during an extended period of time.
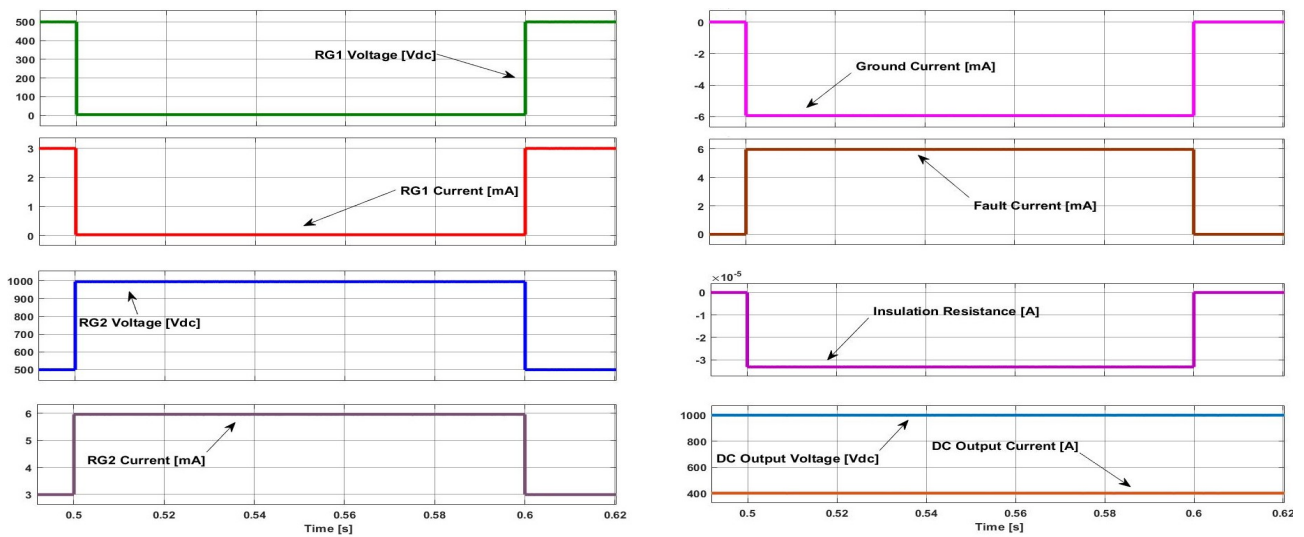
Figure 56: Line-to-ground fault

Figure 57 shows the voltage and current through a human body with respect to the ground, touching the chassis that has become "live" during a LG fault. Since the battery's chassis is energized with a voltage potential of 1000 V, the current through the body will be 0.6 A due to Ohm's law, as stated in equation 9. This current is not safely low enough if a human touches the energized part of the chassis. From this simulation, the ship-side grounding system should have been designed with a EBC, which cancels dangerous voltage potential differences between "live" metal parts when the ground fault occurs. They are employed for connections of EXCPs to the main earthing bus. The main earthing bus links together protective conductors, EBCs, and earthing conductors[11].
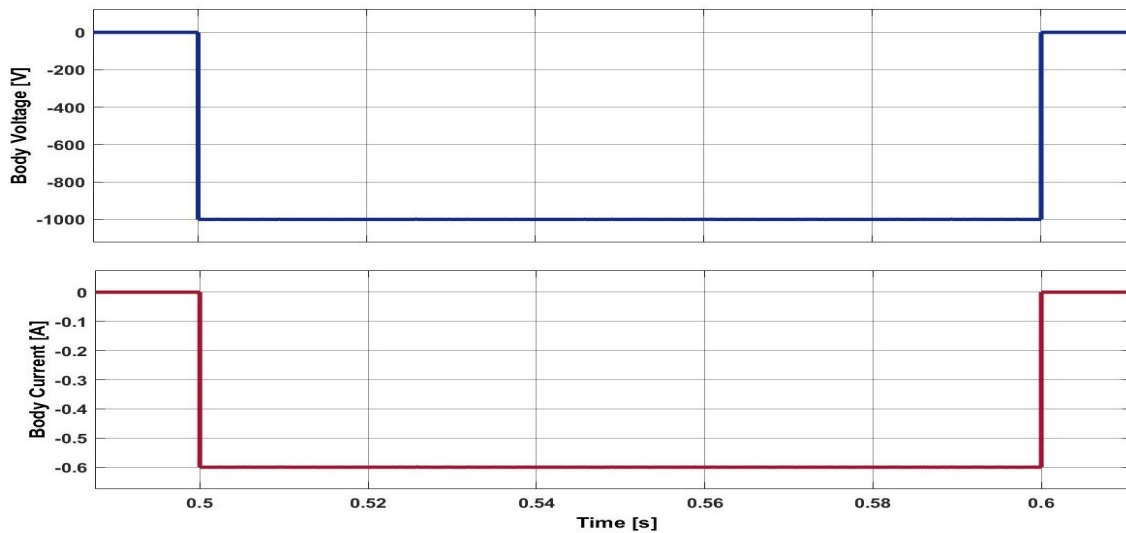
Figure 57: Voltage drop and current through a human body

Line-to-Line Fault

Figure 58 shows the fault current response of the DC-link during a LL fault. The discharge of the DC capacitor results in a transient fault current on the DC-link side, reaching 70 kA peak in a very short period until it keeps stable at a rating current of 4.6 kA. In this type of fault, it is necessary to rapidly clear the fault by fuses or automatic DCCBs, since this is potentially a hazardous situation. The figure also shows the load resistor's (battery's) output voltage and current during a LL fault. The converter's low power response is because of the DC-link voltage that collapsed after the LL fault was introduced. However, it can be concluded that the power system remains safe and stable during a LG fault, but the LG fault leads to voltage potential among the ships and the pier. The LL fault reaches a potentially dangerous situation during a LL fault and must be cleared rapidly in reality.
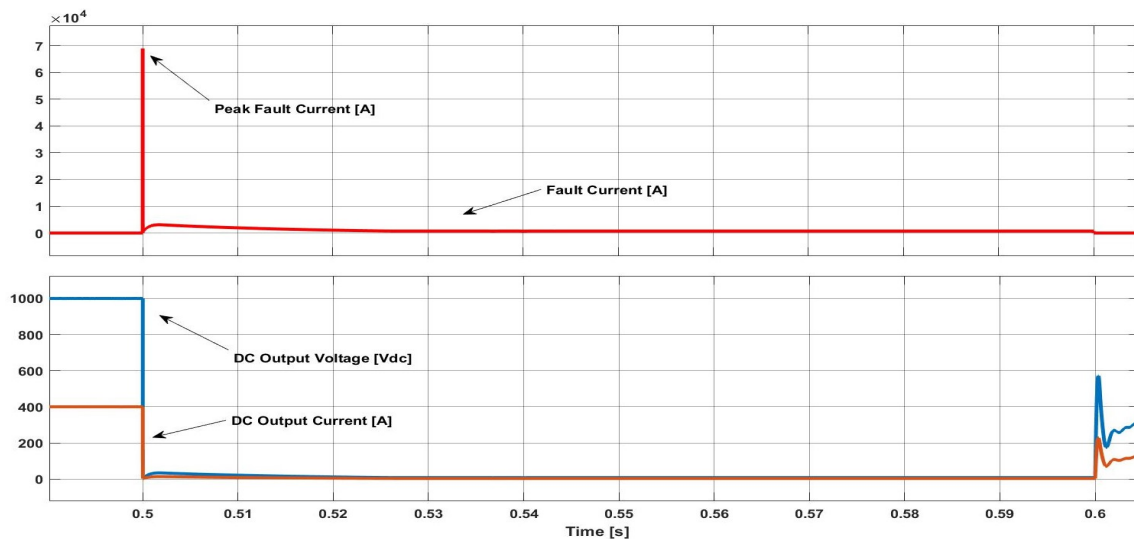
Figure 58: DC link current through a LL fault

5 Conclusion

In this paper, a complete charging and grounding system for cold ironing operation has been proposed and verified in the Matlab/Simulink environment. The simulations confirmed that the complete system worked during normal and fault conditions.

Furthermore, a shore-side TF was designed with a frequency of 50 Hz and with a calculated core loss resistance and magnetizing resistance. The primary and secondary winding parameters were adjusted through simulations to provide enough power to the charging system. In order to convert the AC power to DC power, an uncontrolled three-phase diode bridge rectifier was implemented in the charging system. A derived mid-point of the rectifier's output was obtained through two equal-valued filter capacitors. The voltages across the capacitors aimed voltage balance which was verified through an extended simulation time of 30 s.

The galvanic isolation between the shore and ship-side has been obtained through the design of an ideal 400 kW conventional PSFB DC-DC converter with a nominal output voltage of 1000 V_{dc}. The ideal waveforms of the PSFB DC-DC converter were confirmed through simulations of the HF TF's primary and secondary voltages and currents. The converter reached a stable output during nominal and half load with the designed LC filter parameters and with the control system's PID parameters. The maximum ripple voltage during nominal and half load was 0.15 V and 0.5 mV, respectively. During nominal and half loads, the maximum ripple current was 0.42 A and 0.12 mA. However, the maximum ripple voltage and the current were much lower when the converter was implemented into the complete charging system than during the design process with an ideal voltage source of 800 V_{dc}. When the load resistor of the PSFB DC-DC converter increased to 5 Ω, the DC bus voltage became higher than desired due to the uncontrolled diode bridge rectifier and the shore-side's TF's windings parameters that were adjusted. In addition, the designed phase-shift of 50 % was not achieved, which indicated that the energy transferred is lower than the designed due to the high voltage on the DC bus.

Next, in order to preserve the galvanic isolation between the ships as well as to reduce the leakage current during a ship-side fault, two separate grounding systems were proposed. The shore-side power system was designed as a double grounded configuration with a HR NGR on the AC-side and a TN-C grounding system on the DC-side. Through the neutral point from the rectifier's output, a PEN conductor's rated cable resistance was designed and connected to a common ground point with the NGR. The rectifier suffered from a very high power loss during normal conditions when the PEN conductor was connected to the DC-link midpoint. As a consequence, the performance of the PSFB DC-DC converter would unstable. In order to maintain a stable DC output of the DC-DC converter and reduce the power loss on the DC bus, a resistor of 20 Ω was added to the PEN conductor's resistor during simulations of the complete charging system. The power loss was therefore reduced. During the simulation of faults on the shore-side grounding and charging system, the resistor was removed.

Next, an IT grounding configuration with HRMG resistors connected to earth was designed on the ship-side's DC electrical system such that the leakage current was reduced and the personnel safety was kept at a safe level during a fault. The battery's mechanical chassis were separately connected to PE. The chassis's insulation resistance was set to an arbitrary value after research was completed regarding insulation resistance on lithium-ion batteries.

Furthermore, faults that can appear on the shore-side and ship-side were identified through research, and the

existing faults found are single/double phase-to-ground fault and phase-to-phase fault on the AC-side, and LG and LL fault on the DC-side. The identified faults were implemented into the complete system in Matlab/Simulink to verify if the designed grounding system works properly.

AC faults and DC faults were introduced on the charging and grounding system on the shore-side. During normal operation, voltage potential existed on both the NGR and the PEN conductor due to leakage current from the cable capacitors and the filter capacitors on the DC bus. Such voltage potential is also known as CMV. In reality, the large power dissipation of 1.6 kW is unacceptable with the high current flowing through the PEN conductor. Under a single or double phase-to-ground scenario, it was shown that neither the NGR nor the PEN conductor reduced the fault current to a lower value than 25 A. Almost all of the fault current went through the cable capacitors connected to earth, and the fault current's magnitude was in kA-range. The NGR was therefore not correctly designed. In addition, an isolation between the AC side and the DC side in the form of an isolated rectifier or fuses/CBs should have been considered. As a consequence, the rating of the NGR could be correctly designed, as well as a PEN conductor in series with a LR grounding resistor. This would reduce the power loss during normal operation as well as reducing the LG fault current's magnitude. With an isolated AC/DC rectifier, a fault on the AC side would not have affected the DC side's grounding system and opposite. The simulation of ground faults on the shore-side showed that most of the fault current took the shortest path through the cable capacitors. In conclusion, the proposed grounding system on the shore-side did not reduce the fault current value to a maximum of 25 A on the AC-side.

Moreover, through simulations of a phase-to-phase and LL fault, it was shown that the grounding system does not contribute to leading the fault current to the ground (earth). From the shore-side LG fault, a large current flowed through the PEN conductor such that a sufficiently large amount of fault current can be detected during a LG fault. In reality, disconnecting switches would have been tripped the high fault current such that the fault current does not flow upward the capacitors on the AC-side.

Furthermore, a fault current of 6 mA was obtained on the ship-side's IT grounding system due to the designed values of the HRMG resistors. The HRMG resistors did not contribute to power dissipation during normal operation and no significant power loss under a LG fault. The detection of an eventual LG fault can be difficult to identify since the fault current is limited to such a low value. During a LG fault, the healthy pole handled the full DC voltage, increasing one of the HRMG resistor's voltage potential to twice its rated size. The HRMG resistors should therefore be monitored continuously such that if a LG fault occurs, it can be detected by measuring the voltage across the HRMG resistors. During the LG fault, the leakage current that will flow to the ship hull can circulate on the ship hull, so it is essential to clear the fault as soon as possible.

Moreover, with a body resistance of 800 Ω touching the positive DC line during a LG fault, a touch current was restricted to a safe level of 6 mA. The voltage potential across the body resistance was in a safe value of 4.8 V. However, during the scenario where the person with a body resistance of 1667 Ω touched the battery's mechanical chassis during a LG fault, the touch current was 0.6 A. This was because the chassis was energized with a voltage potential of 1000 V. Therefore, ECP should have been equipped with an EBC so that dangerous voltage potentials could be canceled out. During simulation of a LL fault, it was confirmed that the grounding system did not contribute to reducing the fault current because the fault is not leaded to earth.

6 Further Recommendations

In this section, further recommendations will be presented to improve the charging and grounding system if a major rollout of the grounding system is to take place.

Since the three-phase diode rectifier is an uncontrolled power converter, a rectifier with controllable switches is necessary in order to obtain a constant DC bus voltage of 800 V_{dc}. In addition, an isolated AC/DC rectifier is highly recommended. Hence, a fault can be isolated from the AC input and the DC output. Consequently, the design of the NGR can be obtained since only the falt current's value on the AC-side must be defined. The combination of a NGR and a low-impedance PEN conductor did not contribute to reducing the fault current to a defined value.

Moreover, the PSFB DC-DC is recommended to be designed to obtain ZVS, such that the efficiency can be increased. This can be achieved by adding an energy storage inductor to the HF TF's primary side, also termed as a leakage inductor. As a consequence, the switches can get soft-switching conditions.

The ship-side grounding system should also have been tested with an EBC to indicate if the voltage potential during a LG fault in the battery's chassis can be reduced. The situation is not potentially dangerous for a person touching the energized part if the voltage is reduced.

Since there are several types of fault detection strategies, they should be investigated further to obtain the most proper detection strategy for this type of grounding system. The same goes for DCCBs, since several types exist, and they have their respective benefits and drawbacks. In reality, DCCBs are obligatory in critical parts with the potential to flow high short-circuit currents and endanger the ship's safety[18].

A ship free from leakage current will never be achieved as long as an electrical system is operating and placed on the ship and/or connected to the shore-side grid. As stated in this paper, the leakage current appearing on a ship should always be obtained as lowest as possible. However, when a fault occurs, there is also another protection on the ship that is recommended to minimize the corrosion problems even more due to the potential difference between the ships and the quay. Active or passive cathodic protection is recommended to be installed. Authors in [1] recommend that quays should be equipped with passive cathodic protection in the form of sacrificial anodes. These anodes must be created with a metal that is less noble than the metal of the ship's hull (for example, aluminum or zink), and the anodes must also be in contact with the seawater.

Furthermore, the ships are recommended to be painted and equipped with an active cathodic protection system through ICCP systems. The setpoint of the ICCP is recommended to be lower than -900 mV$_{Ag/AgCl}$ (100 mV$_{Zn}$), but must be consulted with the paint suppliers. This will ensure that the whole hull has a potential lower than -800 mV$_{Ag/AgCl}$), which is the limit for adequate cathodic protection at all time. Nevertheless, a vital notification is that the most effective method to reduce corrosion among the ships and the quay is to minimize the voltage potential.

Corrosion issue on charging ships during cold ironing for AC-powered systems has been investigated on a large scale for many years, and standards have been developed for them, as stated in the theory section. However, DC-distributed charging connected to the utility grid does not have the same standard; only recommendations are proposed. Therefore, in the future, standards and more scientific studies should be developed and investigated on

a large scale. Hence, the risk for accelerated corrosion can be reduced, and safety for personnel can be maintained.

References

[1] E. B. Mehammer, O. E. Kongstein, and A. P. Brede, "Grounding Strategies for High Voltage Shore Connection of Large Passenger Vessels," in *2018 IEEE International Conference on Environment and Electrical Engineering and 2018 IEEE Industrial and Commercial Power Systems Europe (EEEIC / I CPS Europe)*, 2018, pp. 1–6.

[2] G. Parise, R. Lamedica, L. Martirano, A. Ruvio, L. Parise, B. Chavdarian, and C.-L. Su, "TN-Grounding Systems for the Emerging Cold Ironing: Multiple Grounded System vs Island System," in *2018 IEEE International Conference on Environment and Electrical Engineering and 2018 IEEE Industrial and Commercial Power Systems Europe (EEEIC / I CPS Europe)*, 2018, pp. 1–6.

[3] Y. Juan, "Single switch three-phase ac to dc converter with reduced voltage stress and current total harmonic distortion," *IET Power Electronics*, vol. 7, no. 5, pp. 1121–1126, 2014.

[4] J. Mohammadi, F. Badrkhani Ajaei, and G. Stevens, "Grounding the DC Microgrid," *IEEE Transactions on Industry Applications*, vol. 55, no. 5, pp. 4490–4499, 2019.

[5] M. Pourmirasghariyan, S. F. Zarei, and M. Hamzeh, "DC-system grounding: Existing strategies, performance analysis, functional characteristics, technical challenges, and selection criteria - a review," *Electric Power Systems Research*, 2022.

[6] K. Stensaas and M. Stakkestad, "COP26: Her er alt om aarets klimatoppmoete," 2021. [Online]. Available: https://www.fn.no/nyheter/cop26-her-er-alt-om-aarets-klimatoppmoete [Lastet ned: 2022-01-24]

[7] "Fourth IMO Greenhouse Gas Study," *International Maritime Organization*, 2020.

[8] Y. Wang, Z. Yu, J. He, S. Chen, R. Zeng, and B. Zhang, "Performance of Shipboard Medium-Voltage DC System of Various Grounding Modes Under Monopole Ground Fault," *IEEE Transactions on Industry Applications*, vol. 51, no. 6, pp. 5002–5009, 2015.

[9] S. Beheshtaein, R. M. Cuzner, M. Forouzesh, M. Savaghebi, and J. M. Guerrero, "DC Microgrid Protection: A Comprehensive Review," *IEEE Journal of Emerging and Selected Topics in Power Electronics*, p. 1, 2019.

[10] "IEEE Recommended Practice for 1 kV to 35 kV Medium-Voltage DC Power Systems on Ships," *IEEE Std 1709-2018 (Revision of IEEE Std 1709-2010)*, pp. 1–54, 2018.

[11] M. Mitolo, *Electrical Safety of Low-Voltage Systems*, 1st ed. New York: McGraw-Hill, 2009.

[12] M. Benden, "Charging Solution for Ships," Ph.D. dissertation, University of Agder, 2021.

[13] G. Parise, L. Parise, P. Chavdarian, S. Sabatini, and C.-L. Su, "The TN-island system for cold ironing," 2015, pp. 1–6.

[14] M. Kozak and J. Chmiel, "Cold Ironing Galvanic Corrosion Issues with Regard to a Shore-to-Ship Medium Voltage Connection," *Energies*, vol. 13, p. 5372, 2020.

[15] M. Marzinotto, G. Mazzanti, and M. Nervi, "Ground/sea return with electrode systems for HVDC transmission," *International Journal of Electrical Power & Energy Systems*, vol. 100, pp. 222–230, 2018.

[16] J. Nelson, D. O. Burns, R. Seitz, and A. Leoni, "The grounding of marine power systems: problems and solutions," *Fifty-First Annual Conference 2004 Petroleum and Chemical Industry Technical Conference, 2004.*, pp. 151–161, 2004.

[17] F. D'Agostino, S. Grillo, R. Infantino, and E. Pons, "High Voltage Shore Connection Systems: Grounding Resistance Selection and Short Circuit Currents Evaluation," *IEEE Transactions on Transportation Electrification*, pp. 1–10, 2021.

[18] K. Kim, K. Park, G. Roh, and K. Chun, "DC-grid system for ships: a study of benefits and technical considerations," *Journal of International Maritime Safety, Environmental Affairs, and Shipping*, vol. 2, no. 1, pp. 1–12, 2018.

[19] S. Chapman, *Electric machinery fundamentals*, 5th ed. New York: McGraw-Hill, 2012.

[20] OsloEconomics, "Nettkundenes nytte av en oppgradering av lavspenningsnettet," *Norges Vassdrags- og Energidirektorat*, no. 7, 2019.

[21] L. Ringheim, "Grid Impact from Increased Prosumer Penetration in the Norwegian Distribution Grid," *Master's thesis in Energy and Environment*, 2020.

[22] B. Lacroix and R. Calvas, "earthing systems worldwide and evolutions," sep 1995.

[23] K. Satpathi, A. Ukil, and J. Pou, "Short-Circuit Fault Management in DC Electric Ship Propulsion System: Protection Requirements, Review of Existing Technologies and Future Research Trends," *IEEE Transactions on Transportation Electrification*, vol. 4, no. 1, pp. 272–291, 2018.

[24] O. Antoine, L. Papangelis, S. Michels Alfaro, and A. Guittonneau, "Technical Requirements for Connection to Offshore HVDC Grids in the North Sea: Companion Guide," *Directorate-General for Energy Internal Energy Market*, 2020.

[25] V. Staudt, R. Bartelt, and C. Heising, "Fault Scenarios in DC Ship Grids: The advantages and disadvantages of modular multilevel converters." *IEEE Electrification Magazine*, vol. 3, no. 2, pp. 40–48, 2015.

[26] B. Jacobson and J. Walker, "Grounding Considerations for DC and Mixed DC and AC Power Systems," *Naval Engineers Journal*, vol. 119, pp. 49–62, 2007.

[27] D. Paul, "DC traction power system grounding," *IEEE Transactions on Industry Applications*, vol. 38, no. 3, pp. 818–824, 2002.

[28] W. Leterme and D. Hertem, "Classification of Fault Clearing Strategies for HVDC Grids," in *Sweden: CIGRE Symp*, Lund, 2015.

[29] UiA, "Lecture 9: Earthing Schemes- Jording i elektriske installasjoner."

[30] J. Mohammadi, F. B. Ajaei, and G. Stevens, "DC microgrid grounding strategies," in *2018 IEEE/IAS 54th Industrial and Commercial Power Systems Technical Conference (I CPS)*, 2018, pp. 1–6.

[31] R. M. Cuzner, T. Sielicki, A. E. Archibald, and D. A. McFarlin, "Management of ground faults in an ungrounded multi-terminal zonal DC distribution system with auctioneered loads," in *2011 IEEE Electric Ship Technologies Symposium*, 2011, pp. 300–305.

[32] J.-D. Park and J. Candelaria, "Fault Detection and Isolation in Low-Voltage DC-Bus Microgrid System," *IEEE Transactions on Power Delivery*, vol. 28, no. 2, pp. 779–787, 2013.

[33] P. E. Dev Paul and P. B. Chavdarian, "A closer look at the grounding of shore-to-ship power supply system," in *Conference Record 2009 IEEE Industrial Commercial Power Systems Technical Conference*, 2009, pp. 1–7.

[34] L. J. Kingrey, R. D. Painter, and A. S. Locker, "Applying High-Resistance Neutral Grounding in Medium-Voltage Systems," *IEEE Transactions on Industry Applications*, vol. 47, no. 3, pp. 1220–1231, 2011.

[35] "IEEE Recommended Practice for Grounding of Industrial and Commercial Power Systems," *IEEE Std 142-2007 (Revision of IEEE Std 142-1991)*, pp. 1–225, 2007.

[36] "Neutral Grounding Resistors- Technical Information," 2015. [Online]. Available: https://www.postglover.com/wp-content/uploads/downloads/2014/04/NG112-06{_}Technical{_}Information.pdf [Lastet ned: 2022-06-05]

[37] D. Paul, K. L. Peterson, and P. Chavdarian, "Designing Cold Ironing Power Systems: Electrical Safety During Ship Berthing," *IEEE Industry Applications Magazine*, vol. 20, pp. 24–32, 2014.

[38] N. Mohan, *Power Electronics: A First Course*, D. Sayre, Ed.   John Wiley and Sons, Inc, 2012.

[39] H. Patil, "Three-Phase Fault Analysis on Transmission Line in Matlab Simulink," *International Journal for Research in Applied Science and Engineering Technology*, vol. 9, pp. 5386–5391, 2021.

[40] M. Mobarrez, D. Fregosi, S. Bhattacharya, and M. A. Bahmani, "Grounding architectures for enabling ground fault ride-through capability in DC microgrids," in *2017 IEEE Second International Conference on DC Microgrids (ICDCM)*, 2017, pp. 81–87.

[41] M. Carminati and E. Ragaini, "Considerations on DC side grounding configurations of LVDC microgrids," in *2015 5th International Youth Conference on Energy (IYCE)*, 2015, pp. 1–6.

[42] T. Aardalsbakke, "Ground Fault in Shipboard DC Power System," *Master of Science in Electric Power Engineering*, 2015.

[43] J. A. Marrero, "Understand ground fault detection and isolation in DC systems," in *2000 Power Engineering Society Summer Meeting (Cat. No.00CH37134)*, vol. 3, 2000, pp. 1707–1711.

[44] Z. Ali, Y. Terriche, L. Q. N. Hoang, S. Z. Abbas, M. A. Hassan, M. Sadiq, C.-L. Su, and J. M. Guerrero, "Fault Management in DC Microgrids: A Review of Challenges, Countermeasures, and Future Research Trends,"

IEEE Access, vol. 9, pp. 128 032–128 054, 2021.

[45] J.-D. Park, "Ground Fault Detection and Location for Ungrounded DC Traction Power Systems," *IEEE Transactions on Vehicular Technology*, vol. 64, no. 12, pp. 5667–5676, 2015.

[46] C.-H. Lee and C.-J. Lu, "Assessment of grounding schemes on rail potential and stray currents in a DC transit system," *IEEE Transactions on Power Delivery*, vol. 21, no. 4, pp. 1941–1947, 2006.

[47] W. Leterme, P. Tielens, S. De Boeck, and D. Van Hertem, "Overview of Grounding and Configuration Options for Meshed HVDC Grids," *IEEE Transactions on Power Delivery*, vol. 29, no. 6, pp. 2467–2475, 2014.

[48] M. K. Bucher and C. M. Franck, "Comparison of fault currents in multiterminal HVDC grids with different grounding schemes," in *2014 IEEE PES General Meeting — Conference Exposition*, 2014, pp. 1–5.

[49] D. Kumar, F. Zare, and A. Ghosh, "DC Microgrid Technology: System Architectures, AC Grid Interfaces, Grounding Schemes, Power Quality, Communication Networks, Applications, and Standardizations Aspects," *IEEE Access*, vol. 5, pp. 12 230–12 256, 2017.

[50] D. M. Bui, S.-L. Chen, C.-H. Wu, K.-Y. Lien, C.-H. Huang, and K.-K. Jen, "Review on protection coordination strategies and development of an effective protection coordination system for DC microgrid," in *2014 IEEE PES Asia-Pacific Power and Energy Engineering Conference (APPEEC)*, 2014, pp. 1–10.

[51] T. R. de Oliveira, A. S. Bolzon, and P. F. Donoso-Garcia, "Grounding and safety considerations for residential DC microgrids," in *IECON 2014 - 40th Annual Conference of the IEEE Industrial Electronics Society*, 2014, pp. 5526–5532.

[52] T. Dragičević, X. Lu, J. C. Vasquez, and J. M. Guerrero, "DC Microgrids—Part II: A Review of Power Architectures, Applications, and Standardization Issues," *IEEE Transactions on Power Electronics*, vol. 31, no. 5, pp. 3528–3549, 2016.

[53] K. Hirose, T. Tanaka, T. Babasaki, S. Person, O. Foucault, B. J. Sonnenberg, and M. Szpek, "Grounding concept considerations and recommendations for 400VDC distribution system," in *2011 IEEE 33rd International Telecommunications Energy Conference (INTELEC)*, 2011, pp. 1–8.

[54] S. Cui, H.-J. Lee, J.-J. Jung, Y. Lee, and S.-K. Sul, "A Comprehensive AC-Side Single-Line-to-Ground Fault Ride Through Strategy of an MMC-Based HVDC System," *IEEE Journal of Emerging and Selected Topics in Power Electronics*, vol. 6, no. 3, pp. 1021–1031, 2018.

[55] L. Li, J. Yong, L. Zeng, and X. Wang, "Investigation on the system grounding types for low voltage direct current systems," in *2013 IEEE Electrical Power Energy Conference*, 2013, pp. 1–5.

[56] C. Y. Dong, J. H. He, X. K. Wang, J. F. Xu, L. Yu, and Z. Q. Bo, "High-resistance grounding fault detection and location in DC railway system," in *11th IET International Conference on Developments in Power Systems Protection (DPSP 2012)*, 2012, pp. 1–5.

[57] A. Makkieh, A. Emhemed, D. Wang, A. Junyent-Ferre, and G. M. Burt, "Investigation of different system

earthing schemes for protection of low-voltage DC microgrids," *The Journal of Engineering*, vol. 2019, 2019.

[58] T. Baldwin, F. Renovic, L. Saunders, and D. Lubkeman, "Fault locating in ungrounded and high-resistance grounded systems," in *2001 IEEE Industrial and Commercial Power Systems Technical Conference. Conference Record (Cat. No.01CH37226)*, 2001, pp. 163–169.

[59] J. C. Das and R. H. Osman, "Grounding of AC and DC low-voltage and medium-voltage drive systems," *IEEE Transactions on Industry Applications*, vol. 34, no. 1, pp. 205–216, 1998.

[60] S. A. Memon and P. Fromme, "Stray Current Corrosion and Mitigation: A synopsis of the technical methods used in dc transit systems." *IEEE Electrification Magazine*, vol. 2, no. 3, pp. 22–31, 2014.

[61] I. Cotton, C. Charalambous, P. Aylott, and P. Ernst, "Stray Current Control in DC Mass Transit Systems," *IEEE Transactions on Vehicular Technology*, vol. 54, pp. 722–730, 2005.

[62] "Leakage Current Measurement Reference Design for Determining Insulation Resistance," *Texas Instruments*, 2015.

[63] NEK, "NEK410A:2021-Elektriske intallasjoner i skip," 2021.

[64] Y. Zhang, M. Yu, Y. Xia, and W. Wei, "A Comprehensive Suppression Strategy for Common Ground Circulating Current Caused by Grounding Fault in PV Modules," *IEEE Journal of Emerging and Selected Topics in Power Electronics*, vol. 8, no. 3, pp. 3077–3089, 2020.

[65] L. Tang, X. Dong, S. Shi, and Y. Qiu, "A high-speed protection scheme for the DC transmission line of a MMC-HVDC grid," *Electric Power Systems Research*, vol. 168, pp. 81–91, 2019.

[66] M. Parsi, P. Crossley, P. L. Dragotti, and D. Cole, "Wavelet based fault location on power transmission lines using real-world travelling wave data," *Electric Power Systems Research*, vol. 186, pp. 1–8, 2020.

[67] R. Lazzari, L. Piegari, S. Grillo, M. Carminati, E. Ragaini, C. Bossi, and E. Tironi, "Selectivity and security of DC microgrid under line-to-ground fault," *Electric Power Systems Research*, vol. 165, pp. 238–249, 2018.

[68] C. A. Plet and T. C. Green, "Fault response of inverter interfaced distributed generators in grid-connected applications," *Electric Power Systems Research*, vol. 106, pp. 21–28, 2014.

[69] V. Blasko and V. Kaura, "A new mathematical model and control of a three-phase AC-DC voltage source converter," *IEEE Transactions on Power Electronics*, vol. 12, no. 1, pp. 116–123, 1997.

[70] A. R. Prasad, P. Ziogas, and S. Manias, "An Active Power Factor Correction Technique for Three-Phase Diode Rectifiers," *Power Electronics, IEEE Transactions on*, vol. 6, pp. 83–92, 1991.

[71] K. Yao, X. Ruan, C. Zou, and Z. Ye, "Three-phase single-switch boost PFC converter with high input power factor," in *2010 IEEE Energy Conversion Congress and Exposition*, 2010, pp. 2921–2928.

[72] N. Zhou, J. Wang, Q. Wang, and N. Wei, "Measurement-Based Harmonic Modeling of an Electric Vehicle Charging Station Using a Three-Phase Uncontrolled Rectifier," *IEEE Transactions on Smart Grid*, vol. 6,

no. 3, pp. 1332–1340, 2015.

[73] Q. Wang, N. Zhou, J. Wang, and N. Wei, "Harmonic amplification investigation and calculation of electric vehicle charging stations using three-phase uncontrolled rectification chargers," *Electric Power Systems Research*, vol. 123, pp. 174–184, 2015.

[74] M. Rahiminejad, C. Diduch, M. Stevenson, and L. Chang, "Open-circuit fault diagnosis in 3-phase uncontrolled rectifiers," in *2012 3rd IEEE International Symposium on Power Electronics for Distributed Generation Systems (PEDG)*, 2012, pp. 254–259.

[75] S. Pyakuryal and M. A. Matin, "Filter Design for AC to DC Converter," in *International Refereed Journal of Engineering and Science (IRJES)*, vol. 2, no. 6, 2013, pp. 42–49.

[76] A. H. Yazdavar, M. A. Azzouz, and E. F. El-Saadany, "Harmonic Analysis of Three-Phase Diode Bridge Rectifiers Under Unbalanced and Distorted Supply," *IEEE Transactions on Power Delivery*, vol. 35, no. 2, pp. 904–918, 2020.

[77] L. Zhu, "A Novel Soft-Commutating Isolated Boost Full-Bridge ZVS-PWM DC–DC Converter for Bidirectional High Power Applications," *IEEE Transactions on Power Electronics*, vol. 21, no. 2, pp. 422–429, 2006.

[78] I. Alhurayyis, A. Elkhateb, and D. John Morrow, "Isolated and Non-Isolated DC-to-DC Converters for Medium Voltage DC Networks: A Review," *IEEE Journal of Emerging and Selected Topics in Power Electronics*, pp. 1–14, 2020.

[79] M. A. Sakka, J. V. Mierlo, and H. Gualous, "DC/DC Converters for Electric Vehicles," in *Electric Vehicles*, S. Soylu, Ed. Rijeka: IntechOpen, 2011, ch. 13.

[80] Y. Song and J. Niu, "Application of chaotic pulse width modulation control for suppressing electromagnetic interference in a half-bridge converter," *The Journal of Engineering*, vol. 2014, 2014.

[81] R. W. Erickson and D. Maksimović, *Fundamentals of Power Electronics*, 3rd ed. Springer, Cham, 2020.

[82] S. Zhao, J. Zhang, and Y. Shi, "A low cost low power Flyback converter with a simple transformer," in *Proceedings of The 7th International Power Electronics and Motion Control Conference*, vol. 2, 2012, pp. 1336–1342.

[83] A. A. Mohammed and S. M. Nafie, "Flyback converter design for low power application," in *2015 International Conference on Computing, Control, Networking, Electronics and Embedded Systems Engineering (ICCNEEE)*, 2015, pp. 447–450.

[84] B. Tiwari and B. Pal, "Review of Soft Switched Flyback Converters," *INTERNATIONAL JOURNAL OF ENGINEERING RESEARCH & TECHNOLOGY (IJERT) NCETER*, vol. 9, no. 11, 2021.

[85] B. Whitaker, A. Barkley, Z. Cole, B. Passmore, D. Martin, T. R. McNutt, A. B. Lostetter, J. S. Lee, and K. Shiozaki, "A High-Density, High-Efficiency, Isolated On-Board Vehicle Battery Charger Utilizing Silicon Carbide Power Devices," *IEEE Transactions on Power Electronics*, vol. 29, no. 5, pp. 2606–2617, 2014.

[86] A. M. Abou-Alfotouh, A. V. Radun, H.-R. Chang, and C. Winterhalter, "A 1-MHz hard-switched silicon carbide DC–DC converter," *IEEE Transactions on Power Electronics*, vol. 21, no. 4, pp. 880–889, 2006.

[87] J. Biela, M. Schweizer, S. Waffler, and J. W. Kolar, "SiC versus Si—Evaluation of Potentials for Performance Improvement of Inverter and DC–DC Converter Systems by SiC Power Semiconductors," *IEEE Transactions on Industrial Electronics*, vol. 58, no. 7, pp. 2872–2882, 2011.

[88] L. Roggia, F. Beltrame, L. Schuch, and J. R. Pinheiro, "Comparison between full-bridge-forward converter and DAB converter," in *2013 Brazilian Power Electronics Conference*, 2013, pp. 224–229.

[89] Z. Zhang and M. A. E. Andersen, "High frequency AC inductor analysis and design for dual active bridge (DAB) converters," in *2016 IEEE Applied Power Electronics Conference and Exposition (APEC)*, 2016, pp. 1090–1095.

[90] Y. Guo, J. Meng, Y. Wang, and C. Wang, "A Virtual DC Machine Control Strategy for Dual Active Bridge DC-DC Converter," in *2019 IEEE Innovative Smart Grid Technologies - Asia (ISGT Asia)*, 2019, pp. 2384–2388.

[91] J. A. Sabate, V. Vlatkovic, R. B. Ridley, F. C. Lee, and B. H. Cho, "Design considerations for high-voltage high-power full-bridge zero-voltage-switched PWM converter," in *Fifth Annual Proceedings on Applied Power Electronics Conference and Exposition*, 1990, pp. 275–284.

[92] N. Guangqun and H. Xue, "Novel Full-bridge ZVS DC-DC Converter with an Clamp Diodes," *Physics Procedia*, vol. 33, pp. 1964–1970, 2012.

[93] W.-J. Lee, C.-E. Kim, G.-W. Moon, and S.-K. Han, "A New Phase-Shifted Full-Bridge Converter With Voltage-Doubler-Type Rectifier for High-Efficiency PDP Sustaining Power Module," *IEEE Transactions on Industrial Electronics*, vol. 55, no. 6, pp. 2450–2458, 2008.

[94] C.-Y. Lim, J.-K. Han, M.-H. Park, K.-W. Kim, and G.-W. Moon, "Phase-Shifted Full-Bridge DC-DC Converter With High Efficiency and Reduced Output Filter Using Center-Tapped Clamp Circuit," in *2019 IEEE Applied Power Electronics Conference and Exposition (APEC)*, 2019, pp. 1710–1715.

[95] D. Gautam, F. Musavi, M. Edington, W. Eberle, and W. Dunford, "A zero voltage switching full-bridge DC-DC converter for an on-board PHEV battery charger," in *2012 IEEE Transportation Electrification Conference and Expo (ITEC)*, 2012, pp. 1–6.

[96] Y.-K. Lo, C.-Y. Lin, M.-T. Hsieh, and C.-Y. Lin, "Phase-Shifted Full-Bridge Series-Resonant DC-DC Converters for Wide Load Variations," *IEEE Transactions on Industrial Electronics*, vol. 58, no. 6, pp. 2572–2575, 2011.

[97] N. Hassanzadeh, F. Yazdani, S. Haghbin, and T. Thiringer, "Design of a 50 kW Phase-Shifted Full-Bridge Converter Used for Fast Charging Applications," in *2017 IEEE Vehicle Power and Propulsion Conference (VPPC)*, 2017, pp. 1–5.

[98] Y.-S. Shin, C.-S. Kim, and S.-K. Han, "A Pulse-Frequency-Modulated Full-Bridge DC/DC Converter With

Series Boost Capacitor," *IEEE Transactions on Industrial Electronics*, vol. 58, no. 11, pp. 5154–5162, 2011.

[99] Y.-D. Kim, C.-E. Kim, K.-M. Cho, K.-B. Park, and G.-W. Moon, "ZVS phase shift full bridge converter with separated primary winding," in *2009 IEEE Energy Conversion Congress and Exposition*, 2009, pp. 484–489.

[100] A. Mallik and A. Khaligh, "Variable-Switching-Frequency State-Feedback Control of a Phase-Shifted Full-Bridge DC/DC Converter," *IEEE Transactions on Power Electronics*, vol. 32, no. 8, pp. 6523–6531, 2017.

[101] C. Loh, "Phase Shifted Bridge Converter for a High Voltage Application," Ph.D. dissertation, The University of Edinburgh, Edinburgh, 2003.

[102] "Phase-Shifted Full Bridge DC/DC Converter Design Guide," *Texas Instruments*, pp. 1–55, 2014.

[103] W. Phetphimoon and K. Bhumkittipich, "New Design of Phase-Shifted Full-Bridge Power Converter for Photovoltaic Application," 2019.

[104] S. Rahman, "Design of Phase Shifted Full-Bridge Converter with Current Doubler Rectifier," *Infineon Technologies North America (IFNA) Corp.*, vol. 1, 2013.

[105] O. Ibrahim, N. Z. Yahaya, N. Saad, and K. Ahmed, "Design and simulation of phase-shifted full bridge converter for hybrid energy systems," 2016, pp. 1–6.

[106] A. Kouchaki and M. Nymand, "High efficiency three-phase power factor correction rectifier using SiC switches," in *2017 19th European Conference on Power Electronics and Applications (EPE'17 ECCE Europe)*, 2017, pp. 1–10.

[107] S. Haghbin and T. Thiringer, "3.3kW Onboard Battery Chargers for Plug-in Vehicles: Specifications, Topologies and a Practical Example," *International Journal of Electronics and Electrical Engineering*, pp. 9–16, 2016.

[108] S.-H. Ahn, H. J. Ryoo, J.-W. Gong, and S.-R. Jang, "Low-Ripple and High-Precision High-Voltage DC Power Supply for Pulsed Power Applications," *IEEE Transactions on Plasma Science*, vol. 42, pp. 3023–3033, 2014.

[109] G. Costa, "Tuning a PID Controller," *Power Transmission Engineering*, apr 2011.

[110] M. Memari and V. Nakanwagi, "Electrical Insulation in a 400 V Battery Module for Hybrid Vehicles," Master of Science Thesis, Electric Power Engineering, Chalmers University of Technology, 2014.

[111] ISO 16750-2, "Road vehicles- Environmental conditions and testing for electrical and electronic equipment-Part 2: Electrical loads," 2012.

[112] "From mail: Question regarding legal touch voltage and current in AC and DC net," 2022.

[113] "Standard Capacitor Values & Color Codes." [Online]. Available: https://www.rfcafe.com/references/electrical/capacitor-values.htm

[114] "Standard Inductor Values." [Online]. Available: https://www.rfcafe.com/references/electrical/

inductor-values.htm

[115] HELUKABEL, "Current ratings for UL-CSA cables." [Online]. Available: https://www.hitechcontrols.com/ pdf-cable-techinfo/T75-Current-ratings-UL-CSA-cables.pdf [Lastet ned: 2022-03-03]

[116] "Mail regarding values for conductor resistances from Maciej Kozak."

[117] REN, "Prosjektering av jordingsanlegg," pp. 1–47, may 2020.

[118] "Three Phase Fault: Implement programmable phase-to-phase and phase-to-ground fault breaker system - Simulink." [Online]. Available: https://www.mathworks.com/help/physmod/sps/powersys/ref/ threephasefault.html [Lastet ned: 2022-05-11]

Appendix

nominal core c.s.a.* (in mm²)	Copper conductor		Aluminium conductor	
	DC resistance at 20°C	AC resistance at 50 Hz and 90°C	DC resistance at 20°C	AC resistance at 50 Hz and 90°C
16	1,15	1,47	-	-
25	0,727	0,927	-	-
35	0,524	0,668	0,868	1,113
50	0,387	0,494	0,641	0,822
70	0,268	0,342	0,443	0,568
95	0,193	0,247	0,320	0,411
120	0,153	0,196	0,253	0,325
150	0,124	0,160	0,206	0,265
185	0,0991	0,128	0,164	0,212
240	0,0754	0,099	0,125	0,162
300	0,0601	0,080	0,100	0,130
400	0,0470	0,065	0,0778	0,103
500	0,0366	0,053	0,0605	0,082
630	0,0283	0,044	0,0469	0,065
800	-	-	0,0367	0,053

MAX. CONDUCTOR RESISTANCE (in Ω/km)

*) c.s.a. = cross sectional area